NASA Technical Paper 3204

April 1992

Improved Accuracy for Finite Element Structural Analysis via a New Integrated Force Method

Surya N. Patnaik,
Dale A. Hopkins,
Robert A. Aiello,
and Laszlo Berke

NASA

NASA Technical Paper 3204

1992

Improved Accuracy for Finite Element Structural Analysis via a New Integrated Force Method

Surya N. Patnaik
Ohio Aerospace Institute
Brook Park, Ohio

Dale A. Hopkins,
Robert A. Aiello,
and Laszlo Berke
Lewis Research Center
Cleveland, Ohio

National Aeronautics and Space Administration
Office of Management
Scientific and Technical Information Program

Summary

Finite element structural analysis based on the original displacement (stiffness) method has been researched and developed for over three decades. Although today it dominates the scene in terms of routine engineering use, the stiffness method does suffer from certain deficiencies. Various alternate analysis methods, commonly referred to as the mixed and hybrid methods, have been promoted in an attempt to compensate for some of these limitations. In recent years two new methods for finite element analyses of structures, within the framework of the original force method concept, have been introduced. These are termed the "integrated force method" and the "dual integrated force method."

A comparative study was carried out to determine the accuracy of finite element analyses based on the stiffness method, a mixed method, and the new integrated force and dual integrated force methods. The numerical results were obtained with the following software: MSC/NASTRAN and ASKA for the stiffness method; an MHOST implementation for a mixed method; and GIFT for the integrated force methods. For the cases considered, the results indicate that, on an overall basis, the stiffness and mixed methods present some limitations. The stiffness method typically requires a large number of elements in the model to achieve acceptable accuracy. The MHOST mixed method tends to achieve a higher level of accuracy for coarse models than does the stiffness method as implemented by MSC/NASTRAN and ASKA. The two integrated force methods, which bestow simultaneous emphasis on stress equilibrium and strain compatibility, yield accurate solutions with fewer elements in a model. The full potential of these new integrated force methods remains largely unexploited, and they hold the promise of spawning new finite element structural analysis tools.

Introduction and Overview

The field of finite element analysis for structures, based on the original stiffness method and the more contemporary mixed and hybrid methods, has made great strides during the past three decades. General purpose finite element software such as MSC/NASTRAN (ref. 1) and ASKA (ref. 2), based on the stiffness method, and MHOST (ref. 3), based on a mixed-iterative method, are examples of structural analysis tools available today. The current generation of finite element analysis software, coupled with modern computer hardware, provides the capability to solve challenging engineering problems that require extensive numerical calculations. Despite their popularity and prominence, the current finite element analysis methods are not free from deficiencies, and opportunities for improvement appear to exist. In an attempt to compensate for some of the limitations, two new formulations within the framework of force method concepts have been introduced during the past few years. These are termed the "integrated force method" (IFM) and the "dual integrated force method" (IFMD). This report examines the accuracy of finite element structural analysis via the IFM and IFMD versus analysis by the stiffness and the mixed and hybrid methods.

An overall qualitative assessment of the various analysis methods can be attempted from a consideration of the universal equilibrium equations, which represent the force or stress balance conditions. The force equilibrium conditions, in the general context of finite element analysis, give rise to an unsolvable indeterminate system of equations with a greater number of unknown forces than the number of such equations. The equilibrium equations, being indeterminate, cannot be solved for the unknown forces, except for the trivial statically determinate case. Because of the indeterminancy, various alternative methods have been devised for stress analysis of indeterminate structures. The methods available for finite element analysis that are of interest in this study are briefly summarized in the next section. The nomenclature for the analysis method adapted in this paper is based on the primary unknown of the formulation; these unknowns are defined in table I and illustrated in figures 1 and 2.

The Integrated Force Method—A Direct Force Method

In the direct force method all of the internal forces are treated as the primary unknowns and are directly computed by solving a set of simultaneous equations. A solvable system of equations is obtained by augmenting the rectangular system of equilibrium equations with another rectangular system of equations expressed in terms of the same unknown forces. The augmenting system represents the strain compatibility conditions. The total system resulting from the concatenation of the force equilibrium equations and strain compatability conditions is a solvable set of n equations in n unknowns, the solution of which directly yields all n internal forces. This direct force method, which bestows simultaneous emphasis on both the

TABLE I.—METHODS OF STRUCTURAL ANALYSIS AND ASSOCIATED VARIATIONAL FUNCTIONALS

Name of method		Primary variables		Variational functional
Elasticity	Structures	Elasticity	Structures	
Completed Beltrami-Michell formulation	Integrated force method (IFM)	Stresses	Forces	IFM variational functional
Navier formulation	Stiffness method	Displacements	Deflections	Potential energy
Airy formulation	Classical force method	Stress function	Redundants	Complementary energy
Mixed formulation	Reissner method	Stresses and displacements	Forces and deflections	Reissner functional
Total formulation	Washizu method	Stresses, strains, and displacements	Forces, deformations, and deflections	Washizu functional

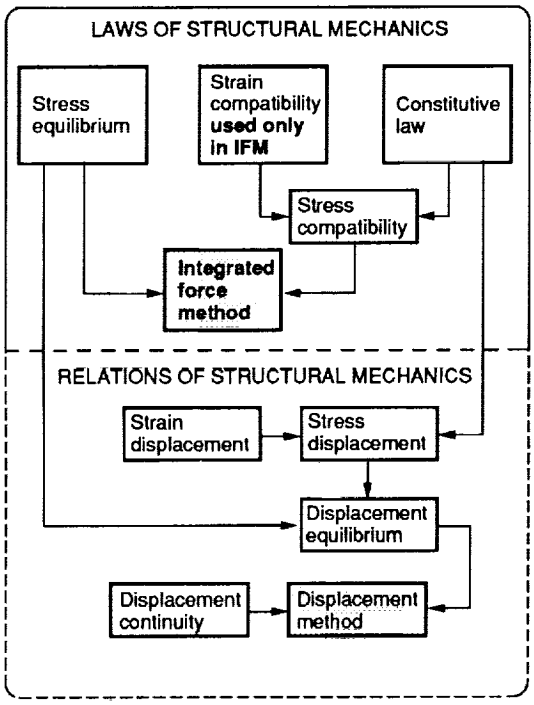

Figure 1.—Force and displacement methods.

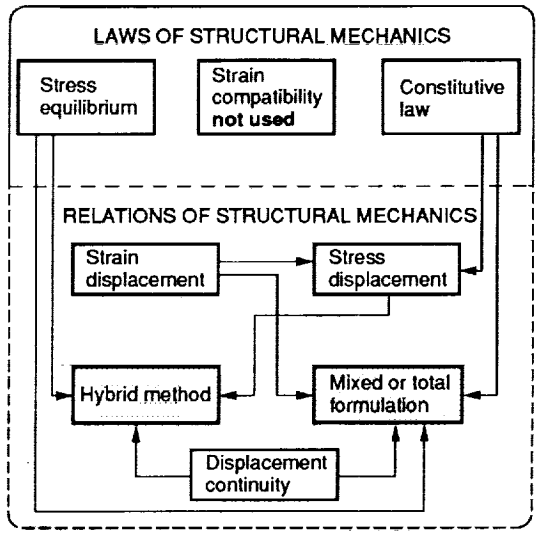

Figure 2.—Hybrid and mixed methods.

equilibrium equations and the compatibility conditions and solves for the forces directly, is the integrated force method (IFM) (refs. 4 to 19). The additional key ingredient for the IFM, which parallels the completed Beltrami-Michell formulation of elasticity (refs. 5, 14, 17, and 20), is the explicit formulation of the global strain compatibility conditions of finite element models. These compatability conditions of finite element models, which are analogous to St. Venant's strain formulation of elasticity, have been divided into interface, cluster, and boundary compatibility conditions (refs. 8, 10, and 11). They enforce deformation balance (1) along the element interface, (2) for a cluster of elements, and (3) along the constrained segment of the boundary of the discrete model. The IFM was not developed in the formative 1960's because the concept of the compatibility conditions augmenting the equilibrium equations for indeterminate structures had not yet been recognized.

Redundant Force Method

Despite the nonavailability of an explicit, computer-automated compatibility formulation, a second classical analysis method, known as the redundant force method (refs. 21 and 22), was developed. The redundant force method was first formulated by Maxwell in the mid 1800's and remained the analysis method of choice for about a century. Recognizing the indeterminate nature of the equilibrium equations, Maxwell introduced the ingenious concept of redundant forces and their use in analysis. In redundant analysis, elements are "cut" to

create a determinate system; then ad hoc compatibility is restored by closing the "gaps". This key procedure yields a system of r equations in terms of r unknown redundant forces. Redundant analysis yields redundant forces that are treated as external loads on the auxiliary determinate structure. The indeterminate analysis is completed by invoking the principle of superposition on the determinant structure.

The redundant force method requires the selection of an auxiliary determinate basis structure and corresponding redundant forces, which is the major difficulty of this classical analysis method. Prior to the availability of computers and the computerization of matrix methods, redundants were identified manually; such a process depended on the subjective experience and judgment of the structural analyst. Subsequently, redundant identification was automated, at least in principle (refs. 23 to 31), on the basis of linear algebra concepts such as rank, column combination and diagonal dominance of the equilibrium matrix, and a self-equilibrating stress state. Such concepts, although analytically elegant, lacked the physical features of the compatibility conditions of finite element models (i.e., deformation balance among element interfaces, clusters, and constrained boundary segments) and the desirable numerical features, such as bandwidth and conditioning of the compatibility matrix. As a result, the redundant force method failed for structures of any complexity. Despite the attention of and earnest efforts by prominent researchers (refs. 23, 25, 27, and 30), the Air Force, and NASA, the redundant force method never became an integral part of the well-known finite element software NASTRAN. The original intent of NASA was to provide for both force and stiffness methods in NASTRAN; however, only the stiffness method implementation now exists.

To illustrate the complexity associated with automatic redundant selection, consider as an example a plate flexure problem (see appendix) in which the plate is discretized by two finite elements and the model has $m = 12$ displacement unknowns and $n = 18$ force unknowns. The maximum possible number of redundant force systems is given by

$$C^r_{\max} = \frac{n!}{(n-m)!m!}$$

or $C^r_{\max} = 49{,}504$ in this case, of which probably only one is the desired canonical set. The maximum possible number of redundant systems from which a canonical set can be selected increases rapidly for more complex structures. For example, for $m = 15$ displacement unknowns and $n = 25$ force unknowns, the maximum number of possible sets exceeds 3 million. Attempts have been made to reduce such large numbers of choices for redundants; however, the problem has not been satisfactorily resolved because of its intrinsically difficult nature. Overall, the classical redundant force method as a computerized method of analysis outlived its usefulness and was abandoned during the early stages of the development of computerized structural analysis technology. Its inclusion in the discussion here is for completeness, but it is not considered further in this study.

Stiffness Method

The statically indeterminate nature of the equilibrium equations and the nonexistence of a strain compatibility formulation led to the direct displacement analysis, or original stiffness, method (ref. 21). In the stiffness method, first formulated by Clebsch (1833 to 1872), the equilibrium equations are written in terms of displacements that when augmented with the displacement continuity conditions give rise to an adequate system of equations with which to solve for the unknown displacements (see the appendix). From the known displacement state, the forces and stress parameters are obtained as secondary variables by differentiation or its equivalent, which could tend to degrade the accuracy of the stress predictions. The stiffness method, which generally requires extensive computations, was not popular until the emergence of high-speed computers. Since the dawn of the computer age (for the past three decades), the stiffness method has been extensively researched throughout the world, and today it dominates the engineering analysis scene.

Mixed and Hybrid Methods

Because of the limitations of the stiffness method, especially with respect to the accuracy of stress solutions, two other approaches have been devised for finite element analysis of structures. The method that considers both stresses and displacements as simultaneous unknowns is referred to as the hybrid method (refs. 31 to 33 and fig. 2). The other method, known as the mixed method (refs. 3 and 34 to 38 and fig. 2), treats displacements, stresses, and strains as simultaneous unknowns. Neither the hybrid nor the mixed method imposes strain compatibility conditions explicitly. Rather, these two methods systematically combine the equilibrium equations, the displacement continuity conditions, the kinematic relations, and the material constitutive relations in one form or another. The hybrid and the mixed methods, although generally more computationally demanding than the direct methods (for comparable discretizations), do not, however, contain any fundamentally new ingredient that is not already present in the force and displacement methods.

The various analysis methods that have been associated with underlying variational functionals are summarized in table I and depicted in figures 1 and 2.

In these figures the following relationships are shown:

(1) The displacement method explicitly utilizes the equilibrium equations written in terms of displacements, which are augmented with the displacement continuity conditions (fig. 1).

(2) The hybrid method includes equilibrium equations, stress displacement relations, and the displacement continuity conditions (fig. 2).

(3) The mixed method uses equilibrium equations, strain displacement relations, the constitutive law, and the displacement continuity conditions. (Note that the equilibrium equations are considered in all the methods.)

(4) The IFM is the only formulation that makes use of the strain compatibility conditions along the interface, field, and boundaries of the finite element model in addition to the equilibrium equations (fig. 1).

(5) The displacement method and the hybrid and mixed methods do not explicitly make use of the strain compatibility conditions (figs. 1 and 2).

If variables are classified with respect to the universal law of equilibrium, then forces are its primal variables, and displacements are its dual variables. On this basis, the IFM is the primal analysis method since its unknowns are the forces, and the stiffness method is the dual method since its unknowns are the displacements. At present, the dual displacement, or stiffness, method has been exhaustively researched, and its potential has been exploited to the extent that the method may have reached a plateau in its development. Conversely, the primal analysis method, with the emergence of the two new integrated force methods, appears to hold considerable potential for further development.

Finite Element Analysis

In the discrete finite element analysis technique, the element characteristics and external loads are lumped at the nodal points of the model, and the governing equations are written with respect to these grid points. The solution obtained by finite element analysis should satisfy the two fundamental axioms of structural mechanics (i.e., the satisfaction of the force equilibrium equations and the compliance of the strain compatibility conditions), at least with reference to the grid points of the model. Even though the stiffness method depends heavily on the state of equilibrium at the nodal points, it is commonly observed that at those very cardinal points stresses recovered from the nodal displacements often violate equilibrium. The mixed method of MHOST attempts to compensate for this limitation through an iterative solution process that equilibrates stresses at the node points. Although stress equilibrium imbalance has been researched, the problems have not been resolved to complete satisfaction. The IFM, in which the internal force parameters are explicitly constrained to simultaneously satisfy both the equilibrium equations and the compatibility conditions with reference to the grid points, is an attempt to obtain accurate stresses even at the nodes of the finite element model.

The purpose of this report is to examine the accuracy of the different methods of finite element analysis. To accomplish this, the results obtained for several test problems by different methods were scrutinized with regard to the relative performance.

Numerical solutions for the test cases were obtained with the following finite element software:

GIFT.—Based on the theories of the IFM and the dual IFMD, GIFT is a modest program developed for research purposes.

MSC/NASTRAN.—This program is one of the most widely used stiffness-method-based codes available today.

MHOST.—Designed especially for nonlinear analysis, this program provides a versatile analysis capability based on a mixed-iterative formulation.

ASKA.—The ASKA program, developed in Europe, is also based on the stiffness method. It is used here mainly for numerical verification with the MSC/NASTRAN code.

Hybrid Method.—Although obtained independent of this study, solutions from a hybrid method using element HMPL5 (ref. 34) are included here for the sake for completeness.

This report does not attempt to elaborate on the theoretical details of the different analysis methods. References 4 to 19 can be examined for representative research results on the theory of the IFM for elastic continua, finite element analysis, and design optimization.

The subject matter of this report is presented in four sections: the basic equations of the analysis; the test cases and results; a discussion of the results; and conclusions. In addition, to illustrate the calculation sequence for the force and the stiffness methods, an example is provided in appendix A. Symbols are defined in appendix B.

Basic Equations of the Methods

This section summarizes the governing equations of the analysis methods investigated here, namely, (1) integrated force method, (2) dual integrated force method, (3) stiffness method, and (4) mixed-iterative method. The equations of the hybrid method are not presented. For detailed examination of the theories of the methods, references 1 to 8, 20, and 21 are suggested.

Integrated Force Method and Dual Integrated Force Method

In the integrated force method (IFM), the internal forces are taken as the primary unknowns and the displacements are obtained by a back calculation operation. The dual integrated force method (IFMD) is derived from the equations of the IFM by eliminating internal forces in favor of displacements. The primal variables of the IFMD are, then, the displacements from which forces are recovered in secondary operations.

In the IFM a discretized structure for the purpose of analysis is designated by attributes (n,m), which denote the number of force and displacement degrees of freedoms, respectively. In the IFM analysis a governing set of n equations is expressed in terms of n unknown internal forces $\{\mathbf{F}\}$. The system of n equations is obtained by augmenting the set of m force equilibrium equations

$$[\mathbf{B}]\{\mathbf{F}\} = \{\mathbf{P}\}$$

with the set of $r = n - m$ strain compatibility conditions

$$[\mathbf{C}][\mathbf{G}]\{\mathbf{F}\} = \{\delta\mathbf{R}\}$$

as follows:

$$\left[\frac{[\mathbf{B}]}{[\mathbf{C}][\mathbf{G}]}\right]\{\mathbf{F}\} = \left\{\frac{\{\mathbf{P}\}}{\{\delta\mathbf{R}\}}\right\} \quad \text{or} \quad [\mathbf{S}]\{\mathbf{F}\} = \{\mathbf{P}^*\} \tag{1}$$

where [B] is the $m\times n$ equilibrium matrix, [C] is the $r\times n$ compatibility matrix, [G] is the $n\times n$ concatenated flexibility matrix that links deformations $\{\beta\}$ to forces {F} as

$$\{\beta\} = [\mathbf{G}]\{\mathbf{F}\}$$

{F} is the $n\times 1$ internal force vector, {P} is the $m\times 1$ external load vector, and $\{\delta\mathbf{R}\}$ is the $r\times 1$ effective initial deformation vector defined by

$$\{\delta\mathbf{R}\} = -[\mathbf{C}]\{\beta_0\}$$

where $\{\beta_0\}$ is the $n\times 1$ initial deformation vector, and [S] is the $n\times n$ IFM governing matrix. The matrices [B], [C], [G], and [S] are banded and have full row ranks of m, r, n, and n, respectively. The solution of equation (1) yields n internal forces. The displacements are obtained from the forces in a back calculation operation expressed as

$$\{\mathbf{X}\} = [\mathbf{J}]\{[\mathbf{G}]\{\mathbf{F}\} + \{\beta_0\}\} \tag{2}$$

where [J] is the deformation coefficient matrix defined as the first $m\times n$ partition of $[[\mathbf{S}]^{-1}]^T$. Equations (1) and (2) represent the two key relations of the IFM for finite element analysis that are needed to calculate the forces and displacements, respectively.

In terms of fundamental operators, an analogy can be made between the IFM and the theory of elasticity (ref. 40). The three fundamental operators of elasticity are (1) the equilibrium operator of Cauchy, which relates stresses to external loads; (2) the compatibility operator of St. Venant, which controls components of strain; and (3) the material constitutive tensor of Hooke, which relates strains to stresses. Likewise, the IFM has three operators that are equivalent to the operators of the elasticity theory. The operators, which become matrices in the context of finite element analysis, are (1) the equilibrium matrix [B], which links internal forces to external loads; (2) the compatibility matrix [C], which governs the deformations; and (3) the flexibility matrix [G], which relates deformations and forces. Both the equilibrium and the compatibility operators of elasticity and the corresponding matrices of the IFM are nonsymmetrical, whereas the material constitutive tensor and the flexibility matrix are symmetrical. Governing operators of other formulations (e.g., Navier's displacement formulation, Airy's stress function formulation, Reissner's hybrid formulation, or the Hu-Washizu's mixed formulation) and the matrices of other discrete analysis methods (such as the stiffness, redundant force, mixed, and hybrid methods) are, in principle, derivable from the basic unsymmetrical operators of elasticity and the matrices of the IFM. Mathematically speaking, the derived operators and matrices of other formulations can possess characteristics (i.e., numerical norms, spectral radii, and stability of equation systems) no more superior than the basic unsymmetrical operators of elasticity theory or matrices of the IFM, even when the derived operators and matrices become symmetric (refs. 6 and 7).

The governing equations of the IFMD are generated from the IFM equations (1) and (2) by mapping forces into displacements and vice versa. The key equation of the IFMD, wherein nodal displacement unknowns {X} become the primary variables and are linked to the external loads {P}, resembles the familiar stiffness equation and is given as

$$[\mathbf{K}_s]\{\mathbf{X}\} = \{\mathbf{P}\} \tag{3}$$

where $[\mathbf{K}_s]$ is a matrix defined by the first $m\times m$ partition of the matrix product $[[\mathbf{S}][\mathbf{G}]^{-1}[\mathbf{S}]^T]$ and is referred to as the pseudo-stiffness matrix.

For the element types that have been formulated to date (including rectangular membrane and flexure elements, triangular membrane and flexure elements, and solid brick and tetrahedral elements), we have observed that, for consistent force and displacement field assumptions, the attributes of the pseudo-stiffness matrix (such as symmetry, dimension, and sparsity) are identical to those of the conventional stiffness matrix [K]. Only the magnitudes of nonzero coefficients of the two matrices [K] and $[\mathbf{K}_s]$ differ.

Once displacements are obtained as the solution to equation (3), forces can be obtained by back calculation as

$$\{\mathbf{F}\} = [\mathbf{G}_J]\{\mathbf{X}\} \tag{4}$$

where the $n\times m$ force coefficient matrix $[\mathbf{G}_J]$ is nonsymmetrical and is defined in terms of the product of the inverse of the concatenated flexibility matrix $[\mathbf{G}]^{-1}$ and the first $n\times m$ partition of the transpose of the IFM governing matrix $[\mathbf{S}]^T$ (defined in eq. (1)). Since the flexibility matrix [G] is the block diagonal concatenation of the corresponding element matrices, its inverse is inexpensive to compute, and calculating forces from displacements by using equation (4) requires only a small fraction of the total computations necessary for the entire analysis.

Since equations (1) and (2) of the IFM are mathematically equivalent to equations (3) and (4) of the IFMD, the forces, displacements, and deformations obtained by either of the methods are identical; thus,

$$\{\mathbf{F}\}_{\text{IFM}} = \{\mathbf{F}\}_{\text{IFMD}} \tag{5a}$$

$$\{\mathbf{X}\}_{\text{IFM}} = \{\mathbf{X}\}_{\text{IFMD}} \tag{5b}$$

$$\{\beta\}_{\text{IFM}} = \{\beta\}_{\text{IFMD}} \tag{5c}$$

The relations given by equation (5) have also been observed numerically; that is, the numerical results obtained for each test case satisfied equation (5) as expected.

The Stiffness Method

The governing equation of the stiffness method, wherein the primary variables $\{\mathbf{X}\}$ (the nodal displacements of the finite element model) are linked to external loads $\{\mathbf{P}\}$ through the stiffness matrix $[\mathbf{K}]$, can be symbolized as

$$[\mathbf{K}]\{\mathbf{X}\} = \{\mathbf{P}\} \tag{6}$$

where $[\mathbf{K}]$ is the symmetrical stiffness matrix of dimension $m \times m$.

Unlike the integrated force technique (eq. (2) or eq. (4)), the stiffness method has no single expression that can be used in calculating stress parameters from displacements by back calculations. The equivalent of differentiation and a series of numerical operations are required to generate the deformation and force variables from the nodal displacements.

The MHOST Mixed-Iterative Method

The MHOST finite element code (refs. 3, 36, and 37) implements a mixed-iterative method derived from an augmented Hu-Washizu variational principle, and it employs an equal-order interpolation of the fields, displacement, strain, and stress, which are represented consistently as nodal variables. The mixed equations of the general Hu-Washizu formulation are augmented with the conventional stiffness equation and solved indirectly; that is, the stiffness equation serves as a preconditioner for the iterative recovery of the mixed solution. This avoids the computational penalty of a direct solution of the mixed equation system in which all three fields are treated as simultaneous unknowns. The governing equations of the MHOST mixed-iterative method are expressed as

$$\begin{bmatrix} [\mathbf{K}] & [0] & [\mathbf{E}_m]^T \\ [0] & [\mathbf{G}_m] & [-\mathbf{C}_m]^T \\ [\mathbf{E}_m] & [-\mathbf{C}_m] & [0] \end{bmatrix} \begin{Bmatrix} \{\mathbf{u}\} \\ \{\epsilon\} \\ \{\sigma\} \end{Bmatrix} = \begin{Bmatrix} \{\mathbf{P} - \mathbf{Ku}\} \\ \{0\} \\ \{0\} \end{Bmatrix} \tag{7}$$

where

$$[\mathbf{E}_m] = \int_\Omega [\mathbf{N}_\sigma]^T [\mathbf{B}] d\Omega \tag{8a}$$

$$[\mathbf{G}_m] = \int_\Omega [\mathbf{N}_\epsilon]^T [\mathbf{D}][\mathbf{N}_\epsilon] d\Omega \tag{8b}$$

$$[\mathbf{C}_m] = \int_\Omega [\mathbf{N}_\sigma]^T [\mathbf{N}_\epsilon] d\Omega \tag{8c}$$

The matrix $[\mathbf{K}]$ is the standard stiffness matrix as in equation (6); $[\mathbf{E}_m]$ is an integrated form of the discrete gradient matrix; $[\mathbf{G}_m]$ is the material elastic constitutive matrix; and $[\mathbf{C}_m]$ is the strain projection matrix. The vectors $\{\mathbf{u}\}$, $\{\epsilon\}$, $\{\sigma\}$, and $\{\mathbf{P}\}$ represent the nodal displacements, strains, stresses, and loads, respectively. The matrices $[\mathbf{N}_\epsilon]$ and $[\mathbf{N}_\sigma]$ comprise the interpolating polynomials (shape functions) for the strain and stress fields, respectively.

The iterative process of the MHOST mixed-iterative strategy is as follows:

Step 1: Initial stiffness solution

$$\{\mathbf{X}\} = [\mathbf{K}]^{-1}\{\mathbf{P}\} \tag{9a}$$

Step 2: Nodal displacement update

$$\{\mathbf{X}\}^{n+1} = \{\mathbf{u}\}^n + [\mathbf{K}]^{-1}\left\{\{\mathbf{P}\} - [\mathbf{E}]^T\{\sigma\}^n\right\} \tag{9b}$$

Step 3: Nodal strain projection

$$\{\epsilon\}^{n+1} = [\mathbf{C}]^{-1}[\mathbf{E}]\{\mathbf{X}\}^{n+1} \tag{9c}$$

Step 4: Nodal stress recovery

$$\{\sigma\}^{n+1} = [\mathbf{C}]^{-T}[\mathbf{G}]\{\epsilon\}^{n+1} \tag{9d}$$

Step 5: Evaluation of the nodal equilibrium residual

$$\{\mathbf{r}\}^{n+1} = \{\mathbf{P}\} - [\mathbf{E}]^T\{\sigma\}^{n+1}\{\mathbf{r}\}^{n+1} = \{\mathbf{P}\} - [\mathbf{E}]^T\{\sigma\}^{n+1} \tag{9e}$$

The process iterates on steps 2 to 5 to reduce the residual vector defined by equation (9e) to an acceptable level.

The initial solution given by equation (9a) is the standard stiffness solution, and in MHOST terminology, it is referred to as the MHOST/uniterated solution. The converged solution from steps 2 to 5 is referred to as the MHOST/iterated solution.

Numerical Results

Numerical results for test problems obtained by different methods are presented in this section. The attributes of the finite elements used by the different software are presented next.

MSC/NASTRAN Elements QUAD–4 and TRIA–3

Four-node QUAD–4 and three-node TRIA–3 elements of MSC/NASTRAN were used in this study, with the displacement degrees of freedom constrained in such a way as to separately obtain the membrane and bending responses. For bending response, the degrees of freedom are restricted to a transverse translation and the two rotations; the QUAD–4, then, is a 12-degree-of-freedom element, and TRIA–3, a

9-degree-of-freedom element. For membrane response, the QUAD–4 element has eight degrees of freedom, that is, two in-plane translations for each of its nodes.

ASKA Elements QUAD–4, TRIB–3, and TUBA–3

The ASKA finite element software also has a QUAD–4 element that was used for this study. The attributes of the QUAD–4 element of ASKA are identical with respect to nodes and degrees of freedom to those of the QUAD–4 element of MSC/NASTRAN. Two triangular elements of the ASKA software were used to examine the difference in performance of higher order elements in finite element calculations. The element TRIB–3 for flexural response has three degrees of freedom per node, consisting of a transverse translation and two rotations. Element TUBA–3 is a higher order triangular element, which for bending response alone has six degrees of freedom per node, consisting of one transverse translation, two rotations, and three curvatures. As will be seen, the increase from three to six degrees of freedom per node did not significantly improve the accuracy in the cases considered.

GIFT Elements PLB4SP, MEMRSP, and PLB3SP

The elements of GIFT software used for this study were the four-node plate-bending element PLB4SP, the three-node plate-bending element PLB3SP, and the four-node membrane element MEMRSP (the same element name is used for both the IFM and the IFMD).

The IFM element PLB4SP has three force degrees of freedom per node, consisting of one shear force and two moments, whereas the IFMD element PLB4SP has three displacement degrees of freedom per node, consisting of a transverse translation and two rotations. The PLB4SP element for IFMD corresponds to the restrained QUAD–4 elements of MSC/NASTRAN and ASKA. The force and displacement degrees of freedom of the PLB4SP elements are depicted in figure 3. Likewise, the restrained three-noded triangular element TRIA–3 of MSC/NASTRAN and the IFM/IFMD element PLB3SP are equivalent; TRIA–3 corresponds to translation along the transverse direction and rotations along the two in-plane axes, whereas the IFM element PLB3SP represents nodal forces along those directions for the IFM element. The MEMRSP element is a four-node rectangular membrane element. For the IFM the MEMRSP element contains two force degrees of freedom per node, representing the two membrane forces along the coordinate axes, and for the IFMD it has two displacement degrees of freedom per node.

MHOST Elements SH75 and PS151

The MHOST element SH75 used in this study is a four-node, bilinear, isoparametric, quadrilateral element based on Reissner-Mindlin plate and shell theory (refs. 3 and 38). It has six displacement degrees of freedom per node (three translations and three rotations). The element is formulated in terms of nine generalized deformations, consisting of strains and curvatures (ϵ_x, ϵ_y, ϵ_z, γ_{xy}, γ_{yz}, γ_{xz}, κ_x, κ_y, k_{xy}), and nine generalized stress resultants (N_x, N_y, N_{xy}, S_{yz}, S_{xz}, M_x, M_y, M_{xy}, ψ_z).

The MHOST plane stress element PS151 is a four-node, bilinear, isoparametric, quadrilateral element based on

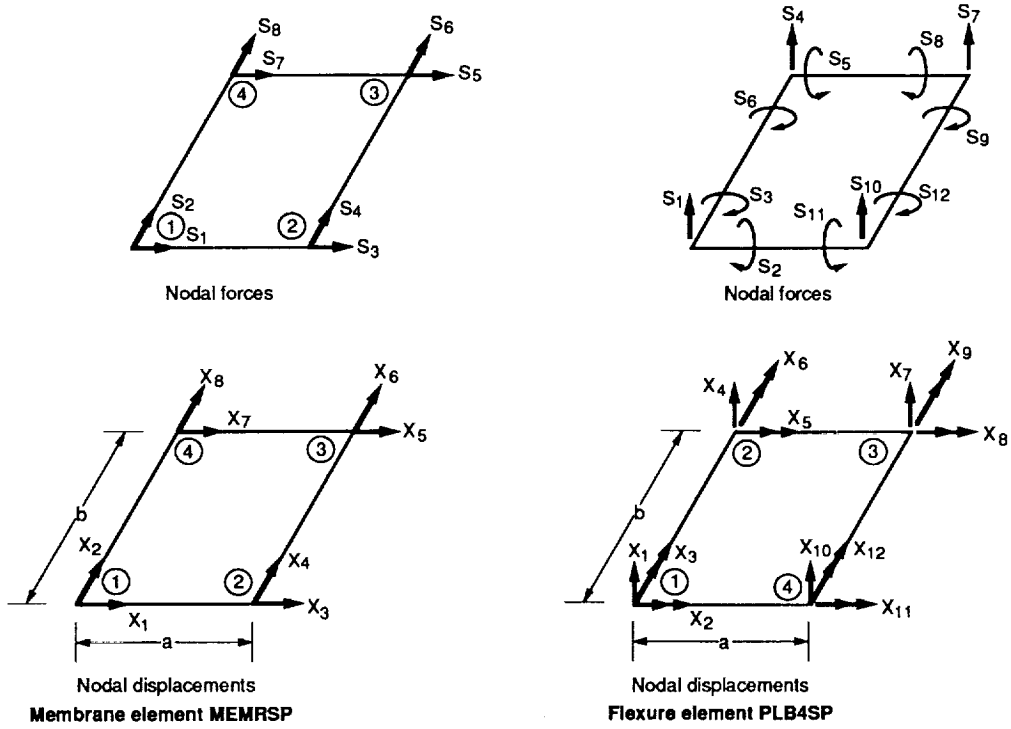

Figure 3.—Four-node membrane and flexure elements.

independent strain interpolation. The nodal variables for the element include two displacements (u_x, u_y), three strains (ϵ_{xx}, ϵ_{yy}, γ_{xy}), and three stresses (σ_{xx}, σ_{yy}, τ_{xy}).

Overall, the elements QUAD-4 and TRIA-3 of MSC/NASTRAN, QUAD-4 and TRIB-3 of ASKA, and PLB4SP, MEMRSP, and PLB3SP of GIFT are "ordinary" elements with three degrees of freedom for bending response and two degrees of freedom for membrane response, and they can be considered equivalent to one another. The elements TUBA-3 of ASKA, and SH75 and PS151 of MHOST can be considered high-precision elements, either because their nodal degrees of freedom exceed those of the normal elements or because an iterative residue-controlling scheme is adopted as in the MHOST/iterative scheme.

The test cases considered for this study are summarized as follows.

Case I—Analysis of the Cantilever Beam

The cantilever beam, shown in figure 4, represents a typical finite element test problem. The beam is made of an isotropic material, and its parameters are as follows:

Length, a, in.	24
Depth, d, in.	2
Thickness, t, in.	0.25
Young's modulus, E, ksi	30 000
Poisson's ratio, ν	0.3
Magnitude of transverse concentrated load at each of two free end nodes, lb	100

The theoretical solutions for the cantilever beam are as follows (ref. 42): displacement at the tip of the beam is

$$\delta y = 0.18432 \text{ in.} \tag{10a}$$

shear force at any location along span x of the beam is

$$\mathbf{V}_y = 200 \text{ lb} \tag{10b}$$

and bending moment along span x of the beam is

$$M_x = 200(24 - x)\text{lb-in.} \tag{10c}$$

The beam was discretized as shown in figure 4(b). It was analyzed by using the quadrilateral elements QUAD-4 of MSC/NASTRAN, element MEMRSP of GIFT, and elements SH75 and PS151 of MHOST. The computed results for displacement and stress were normalized with respect to the theoretical solutions. The displacement and stress results along with the equilibrium imbalance at the nodes of the finite element model are presented in tables II to IX. However, nodal stresses obtained by stiffness methods (MSC/NASTRAN and ASKA) were ambiguous (ref. 39); therefore these are not included in table IV. The convergence of the tip displacement solution with respect to the number of finite elements in the discrete beam model is depicted in figure 5. The stiffness (eq. 6) and the pseudo-stiffness (eq. 3) coefficients for a 12-element model are given in table X.

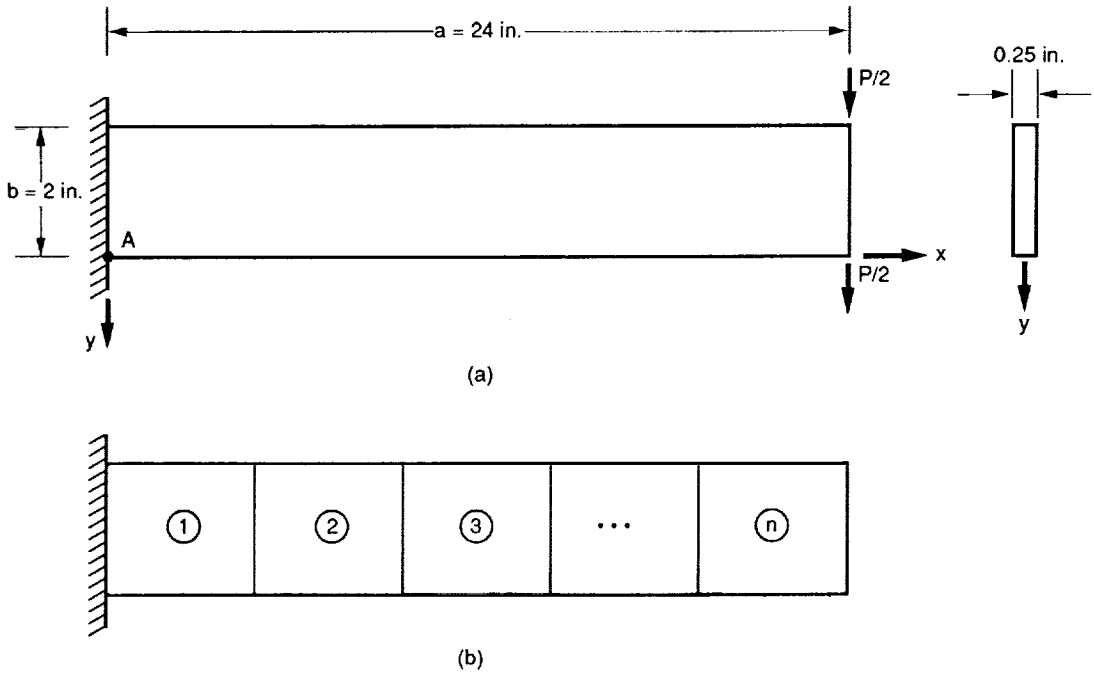

(a) Geometry and boundary conditions.
(b) Finite element model.

Figure 4.—Cantilever beam analysis—Case I.

TABLE II.—COMPARISON OF IFM, MSC/NASTRAN, AND MHOST CANTILEVER BEAM NORMALIZED TIP DISPLACEMENTS[a]

Number of elements, n	Normalized displacement				
	GIFT/IFM MEMRSP	GIFT/IFMD MEMRSP	MSC/NASTRAN QUAD-4	MHOST SH75	
				Uniterated solution	Iterated solution
1	0.755	0.755	0.614	0.678	0.678
2	.942	.942	.858	.855	1.024
3	.977	.977	.889	.888	.955
4	.989	.989	.900	.900	.945
6	.998	.998	.908	.908	.927
8	1.000	1.000	.911	.911	.921
10	1.002	1.002	.912	.912	.919
12	1.002	1.002	.913	.913	.918
16	-----	-----	.914	.914	.914
24	-----	-----	.914	.914	.914
48	-----	-----	.914	.914	.914

[a]Unity represents analytical solution.

TABLE III.—COMPARISON OF IFM AND MHOST ELEMENT PS151 CANTILEVER BEAM NORMALIZED TIP DISPLACEMENTS[a]

Number of elements, n	Normalized displacement			
	GIFT/IFM MEMRSP	GIFT/IFMD MEMRSP	MHOST PS151	
			Uniterated solution	Iterated solution[b]
1	0.755	0.755	0.755	0.755
2	.942	.942	.942	.986
3	.977	.977	.977	.989
4	.989	.989	.989	.994
6	.998	.998	.998	.999
8	1.000	1.000	1.001	1.001
10	1.002	1.002	1.002	1.002
12	1.002	1.002	1.003	1.003
16	-----	-----	1.004	1.004
24	-----	-----	1.004	1.004

[a]Unity represents analytical solution.
[b]For one iteration.

TABLE IV.—COMPARISON OF IFM AND MHOST ELEMENT SH75 CANTILEVER BEAM NORMALIZED STRESSES AT SUPPORT[a]

Number of elements, n	Normalized stress			
	GIFT/IFM MEMRSP	GIFT/IFMD MEMRSP	MHOST SH75	
			Uniterated solution	Iterated solution
1	1.000	1.000	0.494	0.494
2	↓	↓	.748	.995
3			.832	.943
4			.874	.997
6			.916	1.003
8			.937	.985
10			.950	.988
12			.958	.990
16			.969	.982
24			.979	.988

[a]Unity represents analytical solution.

TABLE V.—COMPARISON OF IFM AND MHOST ELEMENT PS151 CANTILEVER BEAM NORMALIZED STRESSES AT SUPPORT[a]

Number of elements, n	Normalized stress			
	GIFT/IFM MEMRSP	GIFT/IFMD MEMRSP	MHOST PS151	
			Uniterated solution	Iterated solution[b]
1	1.000	1.000	0.500	0.500
2	↓	↓	.750	.838
3			.833	.881
4			.875	.912
6			.917	.944
8			.938	.960
10			.950	.969
12			.958	.975
16			.969	.982
24	↓	↓	.979	.988

[a]Unity represents analytical solution.
[b]For one iteration.

TABLE VI.—COMPARISON OF IFM AND MHOST ELEMENT SH75 CANTILEVER BEAM EQUILIBRIUM IMBALANCES AT POINT A[a]

Number of elements, n	Equilibrium imbalance, percent			
	GIFT/IFM MEMRSP	GIFT/IFMD MEMRSP	MHOST SH75	
			Uniterated solution	Iterated solution[b]
2	0	0	49.839	-----
3	↓	↓	12.478	-----
4			8.322	0.104
6			4.994	.515
8			3.567	.380
10			2.774	.312
12			2.270	.263
16			1.664	.825
24	↓	↓	1.085	.518

[a]Unity represents analytical solution.
[b]For one iteration.

TABLE VII.—COMPARISON OF IFM AND MHOST ELEMENT PS151 CANTILEVER BEAM EQUILIBRIUM IMBALANCES AT POINT A[a]

Number of elements, n	Equilibrium imbalance, percent			
	GIFT/IFM MEMRSP	GIFT/IFMD MEMRSP	MHOST PS151	
			Uniterated solution	Iterated solution[b]
2	0	0	0	−5.847
3	↓	↓	↓	1.807
4				1.130
6				0.921
8				.833
10				.752
12				.682
16				.570
24	↓	↓	↓	.424

[a]Unity represents analytical solution.
[b]For one iteration.

TABLE VIII.—IMPROVEMENT IN MHOST ELEMENT SH75 CANTILEVER BEAM SOLUTION

Number of elements, n	Percentage improvement		Computational penalty	
	Support stress	Tip displacement	Number of iterations	Normalized extra time
1	-----	-----	0	----
2	24.70	16.90	2	1.877
3	11.10	6.70	2	1.022
4	12.30	4.50	3	2.400
6	8.70	1.90	5	3.491
8	4.80	1.00	2	2.00
10	3.80	.70	2	2.04
12	3.20	.50	2	2.037
16	1.30	-----	1	1.650
24	-----	-----	1	1.000
Theory	100.0	100.0	--	----

TABLE IX.—IMPROVEMENT IN MHOST ELEMENT PS151 CANTILEVER BEAM SOLUTION

Number of elements, n	Percentage improvement		Computational penalty	
	Support stress	Tip displacement	Number of iterations	Normalized extra time
1	---	---	0	---
2	8.8	4.4	1	1.20
3	4.8	1.2	1	1.33
4	3.7	.5	1	1.23
6	2.7	.1	1	1.33
8	2.2	---	1	1.33
10	1.9	---	1	1.27
12	1.7	---	1	1.29
16	1.3	---	1	1.26
24	.9	---	1	1.37

TABLE X.—CANTILEVER BEAM STIFFNESS MATRIX COEFFICIENTS FOR 12-ELEMENT MODEL OF STIFFNESS MATRIX DIMENSION (48,48)

Stiffness matrix coefficients, K_{ij} (48th row)	GIFT/IFMD (MEMRSP)	MSC/NASTRAN (QUAD-4)	Difference, percent
$K_{48,01}$ to $K_{48,20}$	0	0	0
$K_{48,21}$	-1.339×10^{6}	-1.339×10^{6}	0
$K_{48,22}$	−2.157	−2.095	2.874
$K_{48,23}$	−.103	−.103	0
$K_{48,24}$	−1.964	−2.026	−3.157
$K_{48,25}$ to $K_{48,44}$	0	0	0
$K_{48,45}$	.134	.103	23.134
$K_{48,46}$	.714	.652	8.863
$K_{48,47}$	1.339	−1.339	0
$K_{48,48}$	3.407	3.468	−1.790

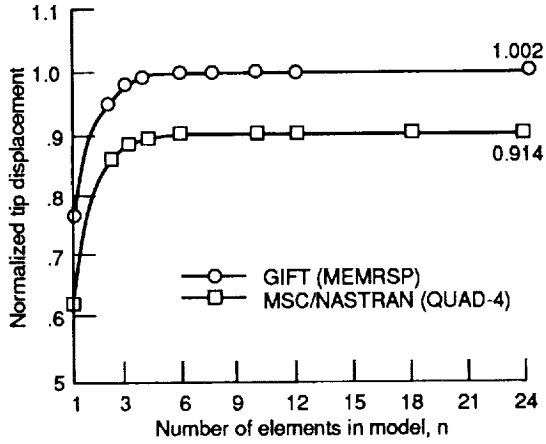

Figure 5.—Convergence of the cantilever beam tip displacement.

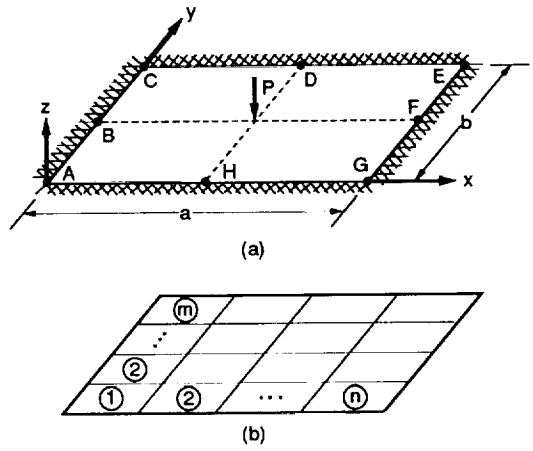

(a) Geometry and boundary conditions.
(b) Finite element model.

Figure 6.—Clamped rectangular plate analysis—Case II.

Case II—Analysis of a Clamped Rectangular Plate

The rectangular plate under a transverse concentrated load, shown in figure 6, represents another typical finite element test problem. The plate is made of an isotropic material, and its parameters are as follows:

Length, a in.	24
Width, b, in.	12
Thickness, h, in.	0.25
Young's modulus, E, ksi	30 000
Poisson's ratio, ν	0.3
Magnitude of transverse concentrated load at center, P, lb	1 000

The plate is clamped, that is, displacements and rotations are restrained, along all four edges. The theoretical solution for the transverse displacement at the center (ref. 41) is

$$\delta_z = 2.42 \times 10^{-3} \text{ in.} \qquad (11)$$

TABLE XI.—COMPARISON OF IFM, MSC/NASTRAN, AND MHOST SH75 NORMALIZED CENTER DISPLACMENTS OF A CLAMPED RECTANGULAR PLATE

Number of elements, ($n \times m$)	Normalized displacement				
	GIFT/IFM PLB4SP	GIFT/IFMD PLB4SP	MSC/NASTRAN QUAD-4	MHOST SH75	
				Uniterated solution	Iterated solution
4 (2×2)	0.825	0.825	0.184	0.006	0.006
8 (4×2)	.987	.987	.306	.010	.010
16 (4×4)	.988	.988	.859	.712	.726
32 (8×4)	1.000	1.000	.945	.833	.858
64 (8×8)	1.000	1.000	.997	.953	.982

TABLE XII.—MHOST SH75 NORMALIZED CENTER DISPLACMENTS FOR SIMPLY SUPPORTED RECTANGULAR PLATE

Number of elements, ($n \times m$)	Normalized displacement	
	Uniterated solution	Iterated solution
4 (2×2)	1.279	-----
8 (4×2)	.739	0.818
16 (4×4)	.806	.997
32 (8×4)	.799	.983
64 (8×8)	.812	.913

TABLE XIII.—COMPARISON OF IFM, MSC/NASTRAN, AND MHOST SH75 NORMALIZED BENDING MOMENTS

Number of elements per quarter plate	Normalized bending moment			
	IFM/IFMD PLB4SP	MSC/NASTRAN QUAD-4	MHOST, SH75	
			Uniterated solution	Iterated solution
1 (1×1)	1.200	0	0	0
4 (2×2)	.994	.787	.620	1.1137
9 (3×3)	.995	.875	.652	.716
16 (4×4)	.995	.931	.732	1.034
25 (5×5)	----	----	.764	.907
36 (6×6)	----	----	.796	.971
49 (7×7)	----	----	.811	.939
64 (8×8)	----	----	.843	.970
81 (9×9)	----	----	.860	.970
100 (10×10)	----	----	.860	.970
400 (20×20)	----	----	.923	.986

The quadrilateral elements of the various software (i.e., PLB4SP of GIFT, QUAD-4 of MSC/NASTRAN, QUAD-4 of ASKA, and SH75 of MHOST) were used to solve the problem. In this case, only the center transverse displacements are compared for the various methods. The normalized values are given in table XI, and the MHOST results obtained for the same plate, but with simply supported boundary conditions, are given in table XII.

Case III—Analysis of a Clamped Square Plate by Quadrilateral Elements

A clamped 24-in. square plate, with other parameters identical to test Case II, was also analyzed by the quadrilateral elements of MSC/NASTRAN, ASKA, GIFT, and MHOST as in Case II. The moment resultant at point B (see fig. 6) as obtained by the different methods is given in table XIII and depicted in figure 7. The transverse center displacements computed by the various methods were qualitatively graded by the criterion proposed by MacNeal and Harder (ref. 42). In their scheme, results are graded as follows on the basis of errors in the nodal displacements:

Grade A less than 2 percent error
Grade B greater than 2 but less than 10 percent error
Grade C greater than 10 but less than 20 percent error
Grade D greater than 20 but less than 50 percent error
Grade F greater than 50 percent error

For Case III, the grades achieved by the different methods are presented in table XIV, and the convergence trend of the center transverse displacement with respect to the number of elements in the model is depicted in figure 8.

Case IV—Analysis of a Clamped Square Plate by Triangular Elements

The computations for the clamped square plate of Case III were repeated with the triangular plate-bending elements PLB3SP of GIFT, TRIA-3 of MSC/NASTRAN, and TRIB-3 and TUBA-3 of ASKA. The TUBA-3 element of ASKA is a higher order element, as described earlier. Results obtained from the different methods were again qualitatively graded according to the MacNeal and Harder criterion. The grades are presented in table XV, and the center transverse displacement convergence trend is depicted in figure 9.

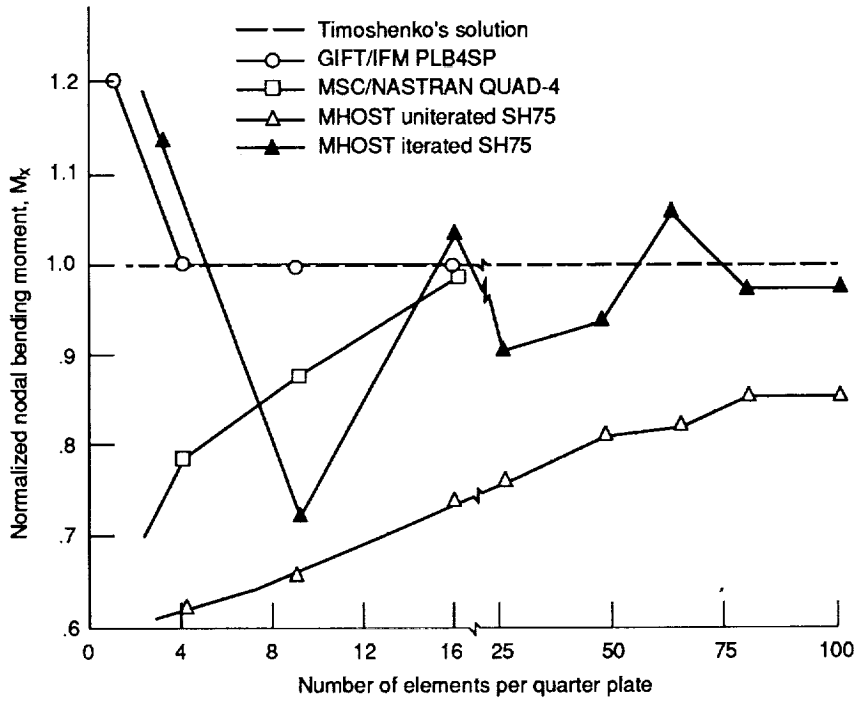

Figure 7.—Convergence of moment for the clamped plate.

TABLE XIV.—REPORT CARD FOR QUADILATERAL ELEMENTS USED TO SOLVE CLAMPED SQUARE PLATE CENTER DISPLACEMENTS

Number of elements for full plate ($n \times m$)	GIFT/IFM GIFT/IFMD (PLB4SP)	MSC/NASTRAN (QUAD-4)	ASKA (QUAD-4)
4 (2×2)	A	F	F
16 (4×4)	A	B	B
36 (6×6)	A	A	—
64 (8×8)	—	A	—
100 (10×10)	—	—	—

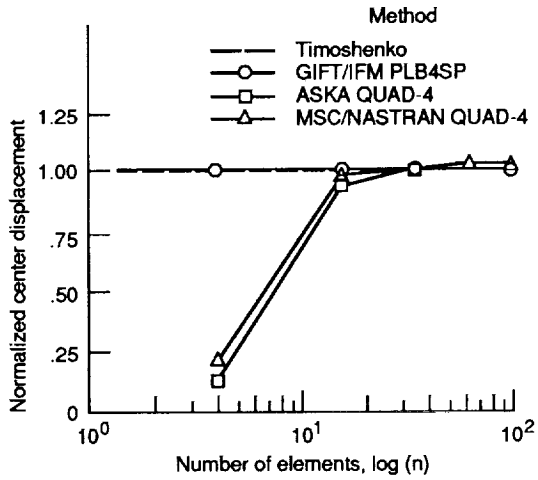

Figure 8.—Rate of convergence for rectangular elements used to calculate clamped square plate transverse center displacement.

TABLE XV.—REPORT CARD FOR TRIANGULAR ELEMENTS USED TO SOLVE CLAMPED SQUARE PLATE CENTER DISPLACEMENTS

Number of elements for full plate	GIFT/IFM GIFT/IFMD (PLB3SP)	MSC/NASTRAN (TRIA-3)	ASKA (TRIB-3)	ASKA (TUBA-3)
4	B	F	—	F
8	A	D	F	F
16	A	C	—	—
32	—	B	C	D
128	—	—	B	B

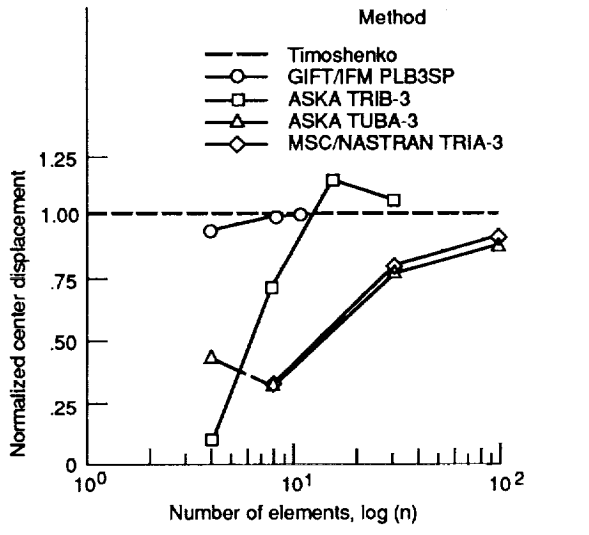

Figure 9.—Rate of convergence for triangular elements used to calculate clamped square plate transverse center displacement.

TABLE XVI.—REPORT CARD FOR IFM RECTANGULAR ELEMENTS WITH DIFFERENT ASPECT RATIOS

Number of elements for full plate ($n \times m$)	Aspect ratio	Clamped boundary	Simply supported boundary
4 (2×2)	1.00	A	A
4 (2×2)	1.20	A	—
	1.40	A	—
	1.60	A	—
	1.80	B	—
	2.00	B	—
8 (2×4)	2.00	A	—
16 (4×4)	1.00	A	A

TABLE XVII.—REPORT CARD FOR HYBRID METHOD RECTANGULAR ELEMENTS ON CLAMPED SQUARE PLATE

Number of elements for full plate ($n \times m$)	GIFT/IFM GIFT/IFMD PLB4SP	Mixed method MHOST SH75	Hybrid method HMPLS [33]
4 (2×2)	A	F	F
16 (4×4)	A	C	C
64 (8×8)	A	B	A

Case V—Analysis of Rectangular Plates With Various Aspect Ratios

Rectangular plates identical to Case II, with both simply supported and clamped boundary conditions and also with different aspect ratios, were examined with the PLB4SP element of the GIFT program. Results are given in table XVI.

Case VI—Analysis of a Clamped Square Plate by the Hybrid Method

This test problem is identical to that of Case IV. The plate was examined with the quadrilateral elements of GIFT and MHOST and the results compared to the hybrid method solution of Chang from element HMPL5 (ref. 33). The qualitative grades achieved by the various methods are given in table XVII.

Discussions

Uniqueness of Elasticity Solution

In the strict mathematical sense, elasticity solutions are unique, that is, for a given force field there is a unique displacement state and vice versa. The IFM and IFMD, being theoretically equivalent, comply with the uniqueness principle (i.e., both IFM and IFMD yield the same solutions; see eq. 5). Although initially the IFM and IFMD results are separately depicted (tables II to XI), thereafter no distinction is made between IFM and IFMD as far as displacement or force solutions are concerned.

Equilibrium Imbalance at the Nodal Points

To examine the extent to which the different analysis methods satisfy the equilibrium conditions at the nodal points of a finite element model, the problem of the cantilever beam in Case I is considered. The normalized equilibrium imbalance at point A (see fig. 4) is defined as

$$I_A = \frac{(F_L - F_R) \times 100}{F_O} \tag{12}$$

where F_L is the member force at point A from the element to the left, F_R is the member force at point A from the element to the right, and F_0 is the theoretical value for the force at point A.

Tables VI and VII show the error (equilibrium imbalance) at point A of the beam model as obtained by GIFT element MEMRSP and MHOST elements SH75 and PS151. The solutions that were obtained by the integrated force methods do not exhibit equilibrium imbalance. The error at point A from the MHOST uniterated solution decreases with an increase in the number of elements in the discretization. It is about 50 percent for the model with 2 elements, but about 1 percent for a relatively fine model with 24 elements. The results of the MHOST iterative scheme, wherein the equilibrium imbalance is reduced by a relaxation process, are given in tables VI and VII. Note that for this case the MHOST iterated scheme has virtually eliminated the error with one iteration. The uniterated scheme of MHOST element PS151 does not exhibit any error at point A; however, the iterated scheme induces minor equilibrium imbalances at that node.

For the plate flexure problems, the nodal equilibrium imbalance is more persistent, especially for the rotational degrees of freedom. For Case II, with a 64-element (8×8) model, an imbalance of zero is observed in the solution obtained by the MSC/NASTRAN QUAD-4 element for the transverse translational degree of freedom. However, for the rotational degree of freedom the nodal imbalance is of the order of magnitude of the reactions developed at the boundary nodes. The solution by the IFM (GIFT, element PLB4SP) for this case does not exhibit any error for either translational or rotational degrees of freedom.

Attributes of the Stiffness and Pseudo-Stiffness Matrices

The attributes of the stiffness and IFMD pseudo-stiffness matrices, given by equations (6) and (3) respectively, are compared for a relatively fine model (i.e., 12 elements) of the cantilever beam test problem. Selected global stiffness coefficients of the MSC/NASTRAN QUAD-4 element and

the pseudo-stiffness coefficients of the GIFT MEMRSP element are given in table X. Both the stiffness matrix [**K**] of the MSC/NASTRAN QUAD–4 element with membrane response only and the pseudo-stiffness matrix [$\mathbf{K}_s$] of the GIFT MEMRSP element are symmetrical—of 8×8 dimension. Both global stiffness matrices retain similar sign and null characteristics. Only the magnitudes of the nonzero coefficients differ; that is, with the exception of two elements, the magnitudes of the other 14 elements of the 48th row of the global stiffness matrix [**K**] are higher than those of the pseudo-stiffness matrix [$\mathbf{K}_s$]. In an overall sense, the stiffness matrix appears to be somewhat "stiffer" than the pseudo-stiffness matrix.

Convergence Trends for Membrane Response

The normalized tip displacements for the cantilever beam of Case I, obtained by GIFT MEMRSP, MSC/NASTRAN QUAD–4, and MHOST SH75, are presented in table II. The displacements are normalized such that unity represents the theoretical solution. For Case I, tip displacement convergence is achieved by GIFT MEMRSP for models with four or more elements. Both MSC/NASTRAN QUAD–4 and MHOST uniterated SH75 converge to approximately 92 percent of the theoretical solution. For fewer elements (less than 8 elements in the model), the MHOST iterated element-SH75 solution is superior to the MSC/NASTRAN and MHOST uniterated solutions. However, neither MSC/NASTRAN QUAD–4 nor MHOST SH75 uniterated or iterated converge at any closer than 92 percent of the closed-form solution, even for a fine, 48-element model. The displacement convergence trends of GIFT MEMRSP and MHOST PS151, given in table III, are identical.

The computed bending stresses at the support of the cantilever beam (point A in fig. 4) for different discretizations, which were obtained by using the MEMRSP element of GIFT and the SH75 and PS151 elements of MHOST, are given in tables IV and V. The results are normalized with respect to the theoretical bending stress, which is given by

$$\sigma_{\text{theoretical}} = \frac{My}{I} \tag{13}$$

where M is the bending moment at the support (4800 in.-lb), y is the distance from neutral plane (1.0 in.), and I is the moment of inertia $\frac{td^3}{12}$ ($=1/6$ in.^{4}).

Both the IFM and IFMD GIFT element MEMRSP yield identical results. Furthermore, the stress result converges for the first model, which has a single element. The mixed method, MHOST, exhibits some error in the computed stress, even for fine models; the MHOST uniterated 24-element SH75 model has an error of 2.1 percent, which is reduced to 1.2 percent by the MHOST iterated solution. The MHOST PS151 results show more rapid convergence, but still require a 16-element model to achieve an error of less than 2 percent. The computational penalty of the MHOST iterated solution (normalized to the MHOST uniterated solution) is shown in table VIII for element SH75 and in table IX for element PS151. The additional computational time required for the iterated solution is one to two times that required for the uniterated solution.

Convergence Trends for Flexure Response

The displacements calculated for the clamped rectangular plate of Case II are presented in table XI. For this problem, GIFT element PLB4SP achieved an accuracy of 98.7 percent for a model with 8 elements (4×2). For a coarser model with only 4 elements (2×2), the error is about 17.5 percent. The solution obtained by MSC/NASTRAN QUAD–4 required 64 elements to achieve an accuracy of 98 percent. For a 64-element SH75 model, the MHOST uniterated solution achieved an accuracy of about 96 percent; the MHOST iterated solution is marginally more accurate. The MHOST results for a simply supported rectangular plate, given in table XII, show good convergence trends, with minor oscillations for the uniterated case.

For the clamped square plate under transverse concentrated load at the center (see table XIV), the ASKA QUAD–4 element achieved results no better than a grade of B, even for a model with 100 elements. The MSC/NASTRAN QUAD–4 element required just 36 elements to produce a "grade A" solution. The GIFT PLB4SP-element solution for the most coarse model, four elements, achieved a grade of A.

The convergence trends of the clamped rectangular plate bending moment M_x at point B (fig. 6), as calculated by GIFT PLB4SP, MSC/NASTRAN QUAD–4, and MHOST SH75, are presented in table XIII and in figure 7. Note that with the GIFT PLB4SP element, convergence for M_x at location B occurs for the second model, which has four elements per quarter plate; the first model, with one element per quarter plate, exhibited a bending moment about 20 percent higher than Timoshenko's theoretical solution. The MSC/NASTRAN QUAD–4 bending moment shows an error of about 7 percent in the fine model with 16 elements per quarter plate. The MHOST uniterated solution exhibits about a 7-percent error for the model with 400 elements per quarter plate (table XIII), but for the same discretization, the MHOST iterated version shows a 2-percent error.

The influence of aspect ratio on the convergence characteristics of a plate flexure problem was examined by the GIFT PLB4SP element. Results, presented in table XVI, show that the accuracy decreases as the aspect ratio of the element increases from unity (square form); however, PLB4SP retains an A grade for the four-element model until the aspect ratio reaches 1.6. For an aspect ratio of 2.0, the whole plate required eight elements to secure a grade of A.

The square plate with clamped boundary was analyzed with triangular elements PLB3SP of GIFT, TRIA–3 of MSC/NASTRAN, and TRIB–3 and TUBA–3 of ASKA. Results are presented in table XV and figure 9. For element PLB3SP, the

result is discernible from the analytical solution for the first model, which has four elements in the whole plate; even so, the results display engineering accuracy. The next model, with eight elements, converges, thereby achieving a grade of A. None of the MSC/NASTRAN QUAD-4 nor the ASKA TRIB-3 and TUBA-3 results could secure a grade of A, even for a finely discretized model with 128 elements, as shown in table XVI.

The displacement convergence characteristics of the IFM and the MHOST mixed and hybrid formulations for a clamped square plate are given in table XVI. The GIFT PLB4SP secured a grade of A for a 4-element model, whereas the HMPL5 hybrid element (ref. 33) secured the same grade only with a 64-element model. The best grade achieved by the MHOST SH75 element for this problem was a B.

Size of Finite Element Models

To solve structural mechanics problems, current finite element applications employ models with a large number of elements and degrees of freedom. Such models are henceforth referred to as large models. Although larger models (which correspond to smaller finite elements) are presumed to yield more accurate solutions, in a strict sense this would be true only when element size shrinks to a point, or the displacement degrees of freedom are infinite, which is beyond computer capability. The question then is, How small should the finite elements be in a particular region of a structure in order to achieve an acceptable level of accuracy in the prediction of stresses and deformations? This question has been researched, and techniques such as adaptive mesh refinements have been developed. Still, no general answer exists, and mesh refinement is largely governed by experience and intuition. A related issue is the large finite element model (with respect to degrees of freedom) whose solution requires thousands of routine calculations. Such a model can be handled with intensive numerical calculations. This is possible because computation has become relatively inexpensive owing to advancements in digital computer technology and because accuracy in numerical calculations has improved. However, when miniaturization is the desirable trend in other disciplines (such as computer science, communication engineering, etc.) should large finite element models from which solutions are extracted by intensive computation be pursued? Perhaps a more appropriate course of action would be to search for accurate modeling techniques that can generate reliable responses with fewer degrees of freedom. The search for such models could be the goal of the next generation of finite element technology.

The issue of model size in finite element calculations is explored by taking the examples of the cantilever beam (Case I) and plate flexure (Case II) problems. The finite element models for the two cases, analyzed by different methods, are depicted in figures 10 and 11. For the cantilever beam, only four GIFT MEMRSP elements were required to secure a grade of A, whereas both MSC/NASTRAN QUAD-4 and MHOST SH75 elements could secure only of grade of B, even for a fine model (see fig. 10). For the plate problem, eight GIFT PLB4SP elements were required to achieve a grade of A. To achieve the same grade, 64 MSC/NASTRAN QUAD-4 elements were needed, whereas 64 MHOST SH75 elements could secure only a grade of B. (Note: For both membrane and flexure response, the GIFT, MSC/NASTRAN, and MHOST elements are equivalent. See NUMERICAL RESULTS.) Overall, the IFM required a much smaller model, and the stiffness and mixed methods a larger model, to achieve an acceptable level of convergence.

Timoshenko used Ritz's displacement method to solve a plate flexure problem with fixed boundary conditions, obtaining accurate solutions with few terms in the series. For the square-plate convergence, Case III, the IFMD required

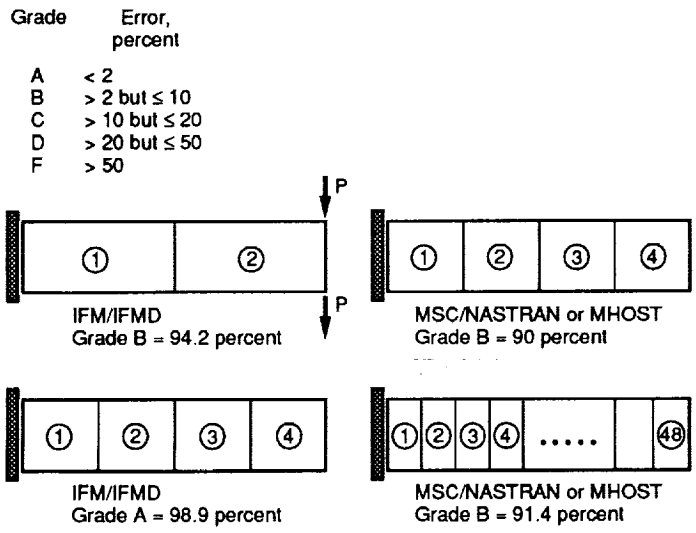

Figure 10.—Number of membrane response elements used for various methods.

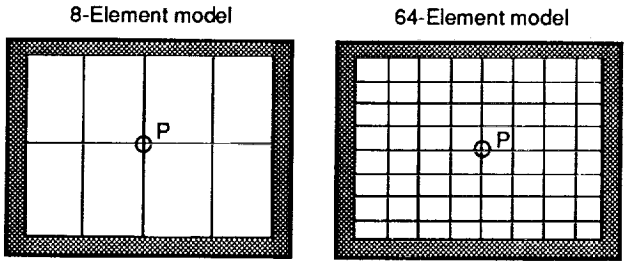

Figure 11.—Number of flexural response elements used for various methods.

four elements with three displacement unknowns. The same problem required 36 MSC/NASTRAN QUAD-4 elements, which corresponds to 75 displacement unknowns. Likewise, 64 or more ASKA QUAD-4 or MHOST SH75 elements, or 64 HMPL5 hybrid elements, all of which correspond to more than 100 variables, were required for convergence. For this plate problem, only IFMD and Ritz's convergence characteristics are similar; that is, both require a similar number of unknowns to achieve convergence.

All of the finite element analysis methods (the IFM, IFMD, stiffness method, hybrid method, and mixed method) are approximate formulations. The solutions obtained by these methods have to be qualified on the basis of indirect criteria such as (1) satisfaction of the equilibrium equations, (2) compliance of the strain compatibility conditions, and (3) elimination of discretization errors by way of the finite element model refinements. The IFM attempts to bestow balanced emphasis on criteria (1) and (2), and it achieves criterion (3) by way of mesh refinement. In other words, all three criteria that qualify the solution (equilibrium, compatibility, and mesh refinement) are incorporated in the IFM; consequently, a converged solution should be accurate and reliable. None of the other formulations (stiffness, hybrid, and mixed) explicitly impose the strain compatibility condition (see figs. 1 and 2); therefore, in a strict sense, there is no guarantee that solutions generated by these methods will always be correct.

Concluding Remarks

Overall, on the basis of the examples analyzed, the following conclusions can be drawn:

1. The integrated force method is superior to the stiffness, mixed, and hybrid methods. The latter three methods all performed at about the same level.

2. Most potentials of the stiffness, hybrid, and mixed methods have been exploited; these methods probably have reached the plateau in their development. The integrated force method has now been established and its potential remains to be explored.

3. Since all of the finite element methods are approximate in nature, we recommend generating solutions both via the integrated force method and the stiffness method and then comparing them, rather than qualifying the results by successive mesh refinements of any one formulation.

Lewis Research Center
National Aeronautics and Space Administration
Cleveland, Ohio, June 12, 1991

Appendix A
A Plate Flexure Example

The solution procedure of the integrated force method (IFM) is illustrated through the example of a flat cantilever plate in flexure (see fig. 12). The plate is made of an isotropic material, has a Young's modulus E of 30 000 ksi, and a Poisson's ratio ν of 0.3. The plate is discretized into two rectangular elements, each of which has three force and three displacement degrees of freedoms per node; the force variables are two moments and a shear force, and the displacement variables are two rotations and a transverse translation (see fig. 3).

Solution by the Integrated Force Method

To analyze the flat cantilever plate by the IFM requires that three matrices be generated: the equilibrium matrix [**B**], the flexibility matrix [**G**], and the compatibility matrix [**C**]. The generation of the matrices is presented in symbolic form to avoid algebraic complexity.

Equilibrium Matrix

The element equilibrium matrix $[\mathbf{B}_e]$ is the transformation that maps nodal loads onto the internal forces at the element level. The element equilibrium matrix is a rectangular matrix; its rows correspond to the displacement degrees of freedom and its columns correspond to independent force variables. The consistent equilibrium matrix is generated from the variational functional of the IFM. The portion of the functional (ref. 5) that yields the matrix $[\mathbf{B}_e]$ can be written as

$$U_{pb} = \int_{\Omega} \left(M_x \frac{\partial^2 w}{\partial x^2} + M_y \frac{\partial^2 w}{\partial y^2} + M_{xy} \frac{\partial^2 w}{\partial x \partial y} \right) dx\, dy \qquad \text{(A1)}$$

where U_{pb} is the strain energy in flexure; M_x, M_y, and M_{xy}

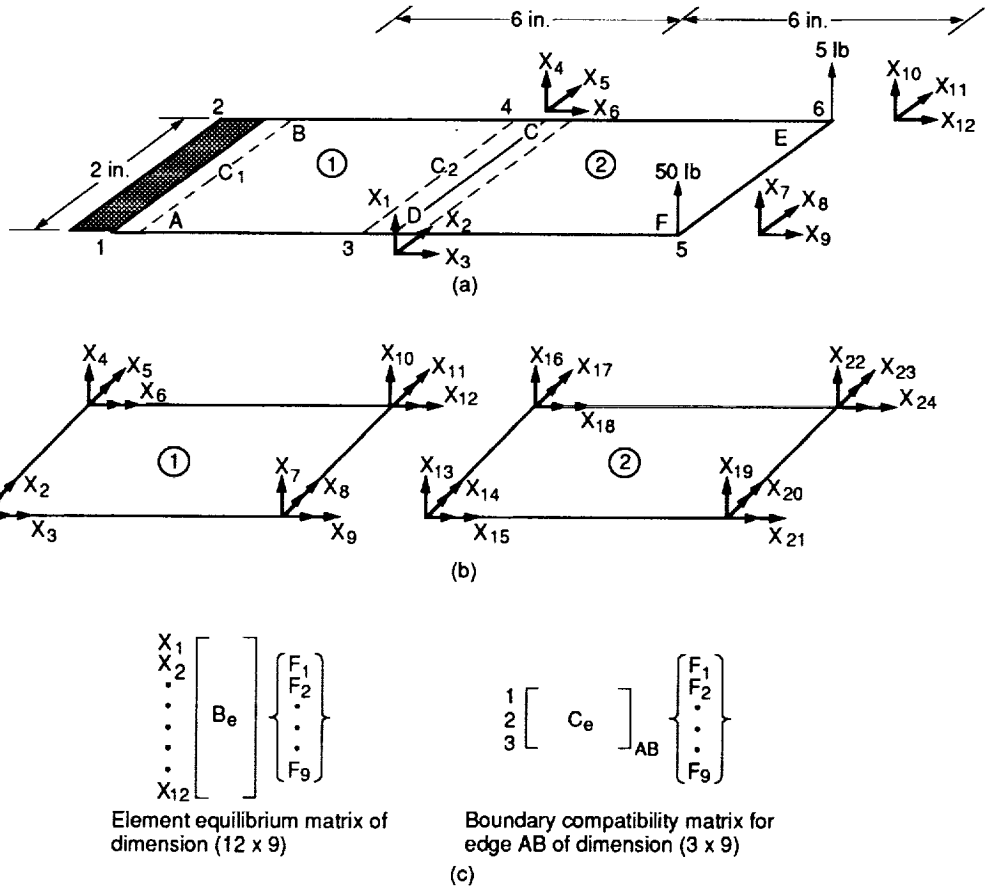

(a) Displacement degrees of freedom.
(b) Concatenated displacement.
(c) Element matrices.

Figure 12.—Flat cantilever plate in flexture.

are the plate-bending moments; and $\frac{\partial^2 w}{\partial x^2}$, $\frac{\partial^2 w}{\partial y^2}$, and $\frac{\partial^2 w}{\partial x \partial y}$, are the plate curvatures.

The plate domain Ω is defined in a rectangular Cartesian coordinate system (x,y).

The discretized internal energy for the rectangular element is expressed as

$$U_{\text{dis}} = \{\mathbf{X}\}^T[\mathbf{B}_e]\{\mathbf{F}\} \tag{A2}$$

where U_{dis} is discretized internal energy for flexural response, $[\mathbf{B}_e]$ is the plate flexure element equilibrium matrix, $\{\mathbf{X}\}$ is the displacement vector of the element, and $\{\mathbf{F}\}$ is the force vector of the element.

The expression to generate a consistent equilibrium matrix $[\mathbf{B}_e]$ is obtained by equating the strain energies given by equations (A1) and (A2):

$$U_{ph} = U_{\text{dis}} \tag{A3}$$

The generation of the consistent element equilibrium matrix $[\mathbf{B}_e]$ requires both the displacement and force distributions in the plate domain. For the displacement field, a polynomial shape function is chosen in terms of 12 unknowns that satisfy the normal plate flexure continuity conditions:

$$w(x,y) = \alpha_1 + \alpha_2 x + \alpha_3 y + \alpha_4 x^2 + \alpha_5 xy + \alpha_6 y^2 + \alpha_7 x^3 + \alpha_8 x^2 y + \alpha_9 x y^2 + \alpha_{10} y^3 + \alpha_{11} x^3 y + \alpha_{12} x y^3 \tag{A4}$$

The 12 constants $(\alpha_1,\alpha_2,\ldots,\alpha_{12})$ of the polynomial are linked to the 12 nodal displacement degrees of freedom $(X_1,X_2,\ldots,X_{12})$ of the element by following standard techniques.

Two mandatory requirements of the assumed force field at the element level are (1) the force field must satisfy the homogeneous equilibrium equation, here, the plate bending equation $\left(\frac{\partial^2 M_x}{\partial x^2} + \frac{\partial^2 M_y}{\partial y^2} + 2\frac{\partial^2 M_{xy}}{\partial x \partial y} = 0\right)$; and (2) the force components F_k (see eq. (A5)) must be independent of one another. The latter condition ensures the kinematic stability of the element. It is not mandatory that the assumed forces satisfy the field compatibility conditions a priori.

The rectangular element can have 12 nodal forces—2 moments and a shear force for each of its 4 nodes. Overall, these 12 force components must satisfy the 3 kinematic equilibrium conditions; in consequence there are only 9 independent forces.

The moment functions of the rectangular element are defined in terms of the nine independent force components as

$$M_x = F_1 + F_2 x + F_3 y + F_4 xy \tag{A5a}$$

$$M_y = F_5 + F_6 x + F_7 y + F_8 xy \tag{A5b}$$

$$M_{xy} = F_9 \tag{A5c}$$

The normal moments vary linearly within the element, whereas the twisting moment is constant. The constant twisting moment M_{xy} will produce interelement discontinuities, which of course, if required, can easily be alleviated by a higher order polynomial. The assumed moments satisfy the previously stated mandatory requirements.

The element equilibrium matrix is obtained by substituting the moments from equation (A5) and the displacements from equation (A4) into the energy expression given by equations (A1) to (A3) and carrying out the integration. The rectangular element equilibrium matrix $[\mathbf{B}_e]$ is of dimension 12×9; its rows correspond to the 12 unknown displacements ($X_1 = W_i, X_2 = \Theta_{xi}$, $X_3 = \Theta_{yi}$ for nodes $i = 1$ to 4) shown in figure 12, and its columns correspond to the 9 independent force unknowns given by equation (A5).

Flexibility Matrix

The element flexibility matrix $[\mathbf{G}_e]$ relates the deformations $\{\beta\}$ to forces $\{\mathbf{F}\}$ as $\{\beta\} = [\mathbf{G}_e]\{\mathbf{F}\}$. The flexibility matrix is symmetrical, of dimension 9×9. It is obtained by following standard techniques to discretize the complementary strain energy U_c, which is given as

$$U_c = (1/2)\{\mathbf{F}\}^T[\mathbf{G}_e]\{\mathbf{F}\} = (1/2D)\int \left[M_x^2 + M_y^2 - 2\nu M_x M_y + (1+\nu)M_{xy}^2\right] dx\, dy \tag{A6}$$

where D is the flexural rigidity defined as $D = (Eh^3/12)$, E is Young's modulus, ν is Poisson's ratio, and h is the plate thickness.

Substituting into equation (A6) the moments M_x,M_y,M_{xy}, in terms of forces $(F_1,F_2,\ldots,F_9)$ as given by equation (A5), and integrating yields the 9×9 symmetric flexibility matrix $[\mathbf{G}_e]$.

Compatibility Matrix

For simplicity, a restrictive procedure to derive the compatibility conditions, which is adequate for the plate flexure problem, is given here. Generating the compatibility matrix, unfortunately, is not as straightforward as generating the equilibrium or the flexibility matrices. Refer to references 8, 10, and 11 for the generation of the compatibility conditions for finite element analysis.

The procedure presented here involves direct discretization of the continuum plate boundary compatibility conditions by using Green's theorem (ref. 43) and Galerkian's technique. The equation form of the compatibility conditions depends on whether such conditions are written for the field or the boundary of the elastic domain, since the compatibility principle is unique. The field compatibility conditions are incorporated into the field integral portion of Green's theorem, and the correspond-

ing boundary compatibility conditions are recovered from the boundary integral portion. The Green's theorem in two dimensions can be written as

$$\int\int_{\Omega}\left[\frac{\partial\phi}{\partial x}+\frac{\partial\psi}{\partial y}\right]dx\,dy=\oint_{\Gamma}[\phi\ell+\psi m]d\ell \qquad \text{(A7)}$$

where ℓ and m are the direction cosines to the outward normal to the boundary curve. The symbols ϕ and ψ represent continuous and differentiable functions of coordinates x and y.

The plate flexure problem is two-degree indeterminate since it has three unknown moments (M_x,M_y,M_{xy}) but only one field equilibrium equation, which is given by

$$\frac{\partial^2 M_x}{\partial x^2}+\frac{\partial^2 M_y}{\partial y^2}+2\frac{\partial^2 M_{xy}}{\partial x\partial y}=q \qquad \text{(A8a)}$$

where q is the transverse distributed load. The problem has two field compatibility conditions (refs. 5 and 17) given by

$$\frac{\partial(M_y-\nu M_x)}{\partial x}-\frac{(1+\nu)\partial M_{xy}}{\partial y}=0 \qquad \text{(A8b)}$$

$$\frac{\partial(M_y-\nu M_y)}{\partial y}-\frac{(1+\nu)\partial M_{xy}}{\partial x}=0 \qquad \text{(A8c)}$$

When Green's theorem is applied to each of these two field compatibility conditions, two boundary compatibility conditions are recovered:

$$(M_y-\nu M_x)\ell-(1+\nu)M_{xy}m=0 \qquad \text{(A9a)}$$

$$(M_x-\nu M_y)m-(1-\nu)M_{xy}\ell=0 \qquad \text{(A9b)}$$

The conditions, specialized for the boundaries of the rectangular element, have the following forms:

1. Along the edges where X = constant, $\ell=1$, and $m=0$,

$$(M_y-\nu M_x)=0 \qquad \text{(A10a)}$$

$$(M_{xy})=0 \qquad \text{(A10b)}$$

2. Along the edges where Y = constant, $\ell=0$, and $m=1$,

$$(M_x-\nu M_x)=0 \qquad \text{(A11a)}$$

$$(M_{xy})=0 \qquad \text{(A11b)}$$

The element compatibility conditions in symbolic form are obtained by substituting the moment functions (eq. (A5)) into the boundary compatibility conditions (eq. (A11)).

Along the edge where Y = constant, $\ell=0$, and $m=1$, the condition given by equation (A11a) yields two equations:

$$(F_1+F_3b)-\nu(F_3+F_7b)=0 \qquad \text{(A12a)}$$

$$(F_2+F_4b)-\nu(F_6+F_8b)=0 \qquad \text{(A12a)}$$

The condition given by eq. (A11b) yields one equation:

$$M_9=0 \qquad \text{(A12c)}$$

The three compatibility conditions given by equation (A12) are representative only in the context of discrete finite element analysis, because lumped nodal quantities and Galerkian integration has not been carried out. The intention here is to demonstrate that there are three compatibility conditions per edge of the element. The element compatibility condition for the edge can be written in matrix form as

$$[\mathbf{C}_e]\{\mathbf{F}\}=\{0\} \qquad \text{(A13)}$$

where $[\mathbf{C}_e]$ is the 3×9 element boundary compatibility matrix for the edge where Y is constant.

Similar compatibility conditions can be written for the element boundary where X is constant, $\ell=1$, and $m=0$. The boundary compatibility equation given by equation (A13) is in terms of nine independent forces $\{\mathbf{F}\}$; it represents the composite compatibility conditions ($[\mathbf{C}][\mathbf{G}]\{\mathbf{F}\}$, where $[\mathbf{C}_e]=[\mathbf{C}][\mathbf{G}]$), of the IFM for finite element analysis. In the computer code GIFT, however, the compatibility matrix $[\mathbf{C}]$ and the flexibility matrix $[\mathbf{G}]$ are generated separately, and their product is explicitly determined. The compatibility conditions given by equation (A13), and those obtained by generating $[\mathbf{C}]$ and $[\mathbf{G}]$ separately and taking their product $[\mathbf{C}][\mathbf{G}]$, will have similar characteristics such as bandwidth and sparsity, but may be different with respect to some scaling factors.

Integrated Force Method Equations for the Problem

Each element has 9 independent unknown forces; therefore the 2-element discretization has 18 force unknowns $\left\{\begin{matrix}\{\mathbf{F}_1\}\\ \{\mathbf{F}_2\}\end{matrix}\right\}$, which represent the concatenation of the element forces as

$$\left\{\begin{matrix}\{\mathbf{F}_1\}^T\\ \{\mathbf{F}_2\}\end{matrix}\right\}=\langle F_1=F_{1e1},\ldots,F_{12}=F_{9e1}:F_{10}=F_{1e2},\ldots,F_{18}=F_{9e2}\rangle \qquad \text{(A14)}$$

where the subscript iej indicates the ith force of element j.

The governing equation $[\mathbf{S}]\{\mathbf{F}\}=\{\mathbf{P}\}$ for the problem is presented next, in equation (A15). Equation (A15) contains

a total of 18 equations, consisting of 12 equilibrium equations (EE) and 6 compatibility conditions (CC), from which the 18 unknowns can be computed:

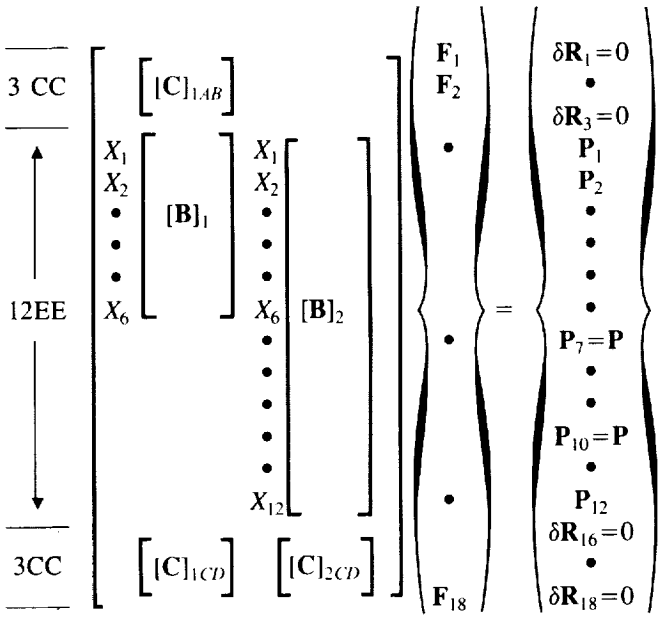

(A15)

where

$[\mathbf{B}]_i$	equilibrium matrix of dimension 12×9 for element i
$P_1, P_2, \ldots, P_{12}$	12-component mechanical loads
$(\delta\mathbf{R}_1, \delta\mathbf{R}_2, \delta\mathbf{R}_3, \delta\mathbf{R}_{16}, \delta\mathbf{R}_{17}, \delta\mathbf{R}_{18})$	6-component initial loads
$[\mathbf{C}]_{iAB}$	edge AB elemental compatibility matrix of dimension 3×9 for element i

The 12 equilibrium equations which link the 18 unknown forces $\left\{\frac{\{\mathbf{F}_1\}}{\{\mathbf{F}_2\}}\right\}$ to the 12 external loads $\{\mathbf{P}\}$ are assembled from the element matrices. The rectangular system of 12 equilibrium equations has the form

$$[[\mathbf{B}_1]:[\mathbf{B}_2]]\left\{\frac{\{\mathbf{F}_1\}}{\{\mathbf{F}_2\}}\right\} = \{\mathbf{P}\} \tag{A16}$$

The 12 system equilibrium equations given by equation (A16) occupy the central portion in the IFM governing equations given by equation (A15).

Because there are 18 force unknowns but only 12 equilibrium equations are available, the plate flexure problem requires 6 compatibility conditions. These six conditions can be identified as the three compatibility constraints along the plate's fixed boundary AB for element 1 and three deformation balance conditions for the boundary CD that is common to both elements 1 and 2 (fig. 12).

The three compatibility conditions along boundary AB can be written in symbolic form as

$$[\mathbf{C}_1]\{\mathbf{F}_1\} = 0 \tag{A17}$$

The matrix $[\mathbf{C}_1]$ has a dimension of 3×9 and is obtained by appropriate substitution of direction cosines of equation (A13) for element 1. These three compatibility conditions occupy the top position in the IFM governing equation depicted in equation (A15).

The three compatibility conditions for the common boundary CD are given by equation (A18). The composite compatibility matrix $[[\mathbf{C}_1]:[\mathbf{C}_2]]$ has a dimension of 3×18 and is obtained from element matrices with appropriate assembly for the edge CD that is common to elements 1 and 2 (see fig. 12).

$$[[\mathbf{C}_1]:[\mathbf{C}_2]]\left\{\frac{\{\mathbf{F}_1\}}{\{\mathbf{F}_2\}}\right\} = \{0\} \tag{A18}$$

The compatibility condition along interface CD is at the bottom location in the IFM governing equation (eq. (A15)). The solution of this governing equation, which contains 12 EE's and 6 CC's, yields the 18 unknown forces. The 12 displacements can then be obtained from the forces by back substitution into equation (2) of the IFM.

The two-element, finite element solution for the plate flexure problem is given in table XVIII along with the strength of material beam solutions, which are obtained from a beam idealization. Note that the two-element solution yields correct moments that are continuous along the interelement boundary CD. The maximum transverse displacement obtained for the two-element model has only 4.5-percent error compared to the theoretical beam solution.

Solution by the Stiffness Method

The cantilever plate flexure problem was also solved by the stiffness method for the purpose of comparison. The stiffness equations are well-known but complicated; therefore, as before, the analysis is carried out in symbolic form. To establish parallelism between the integrated force and the stiffness methods, a slightly different procedure from the normal is followed; the purpose will become evident in the process of the solution. For the problem, a displacement vector $\{\mathbf{X}_c\}$ of dimension 24, which represents the concatenation of the 2 element displacement degrees of freedom, is defined as

$$\{\mathbf{X}_c\} = \langle \mathbf{X}_{c1} = \mathbf{X}_{1e1}, \ldots, \mathbf{X}_{c12} = \mathbf{X}_{12e1} : \mathbf{X}_{c13} = \mathbf{X}_{1e2}, \ldots, \mathbf{X}_{c24} = \mathbf{X}_{12e2} \rangle \tag{A19}$$

TABLE XVIII.—BENDING MOMENTS FOR CANTILEVER BEAM
[See Fig. 12.]

Nodes	Deflection,[a] in.	M_x element 1,[a] in.-lb	M_x element 2, in.-lb	M_y element 1, in.-lb	M_y element 2, in.-lb
1	-----	600.0 (600.0)	-----	378.5	----
2	-----	600.0 (600.0)	-----	378.5	----
3	.2138	−300.0	+300.0	58.60	−58.60
4	.2138	−300.0	+300.0	58.60	−58.60
5	.7048 (.7328)	----- -----	0	-----	----
6	.7048 (.7328)	----- -----	0	-----	----

[a]Quantities in parentheses are from the beam solution.

where the subscript *iej* represents the *i*th displacement for the *j*th element (see fig. 12(c)).

Notice the similarities between the displacement vector $\{\mathbf{X}_c\}$ given by equation (A19) and the force vector $\{\mathbf{F}\}$ given by equation (A15). These vectors ($\{\mathbf{X}_c\}$ and $\{\mathbf{F}\}$) represent the concatenation of the element displacement and force degrees of freedoms, respectively. By following standard techniques, the equilibrium equations given by equation (A18) can be written in terms of nodal displacements $\{\mathbf{X}_c\}$ as

$$[[\mathbf{K}_1]:[\mathbf{K}_2]]\{\mathbf{X}_c\} = \{\mathbf{P}\} \tag{A20}$$

The stiffness matrix $[\mathbf{K}_1]$ is of dimension 6×12, and its six rows represent the contributions to the system equilibrium at nodes 3 and 4 (fig. 12). Likewise, the stiffness matrix $[\mathbf{K}_2]$ is of dimension 12×12, and its 12 rows represent the contributions to the system equilibrium at nodes 3, 4, 5, and 6. The equilibrium equations (eq. (A20)) expressed in terms of displacements still represent an indeterminate rectangular system with 12 equations in terms of 24 unknown displacement variables. Twelve displacement continuity conditions are required to augment the equilibrium equations to a solvable set of 24 equations in 24 unknowns. The 12 displacement continuity conditions for the 2-element plate flexure problem are as follows:

$$X_{c1} = X_{1e1} = 0 \tag{A21a}$$

$$X_{c2} = X_{1e2} = 0 \tag{A21b}$$

$$X_{c3} = X_{1e3} = 0 \tag{A21c}$$

$$X_{c4} = X_{1e4} = 0 \tag{A21d}$$

$$X_{c5} = X_{1e5} = 0 \tag{A21e}$$

$$X_{c6} = X_{1e6} = 0 \tag{A21f}$$

$$X_{c7} = X_{1e7} = X_{2e4} \tag{A21g}$$

$$X_{c8} = X_{1e8} = X_{2e5} \tag{A21h}$$

$$X_{c9} = X_{1e9} = X_{2e6} \tag{A21i}$$

$$X_{c10} = X_{1e10} = X_{2e1} \tag{A21j}$$

$$X_{c11} = X_{1e11} = X_{2e2} \tag{A21k}$$

$$X_{c12} = X_{1e12} = X_{2e3} \tag{A21l}$$

The 12 displacement continuity conditions given by equation (A21) can be represented by a single matrix equation:

$$[\mathbf{C}_{\tau\gamma}]\{\mathbf{X}_c\} = \{0\} \tag{A22}$$

where $[\mathbf{C}_{\tau\gamma}]$ represents the 12×24 displacement continuity matrix. The 12 equilibrium equations (eq. (A20)), written in terms of displacements, are coupled to the 12 displacement continuity conditions (eq. (A21)) to obtain the 24×24 solvable equation system (given by eq. (A23)) of the stiffness method. From this system the 24 displacement components $\{\mathbf{X}_c\}$ can be calculated:

$$\left[\frac{[\mathbf{K}_1]:[\mathbf{K}_2]}{[\mathbf{C}_{\tau\gamma}]}\right]\{\mathbf{X}_c\} = \begin{Bmatrix} P \\ \overline{0} \end{Bmatrix} \tag{A23}$$

The solution of equation (A23), which represents a square but nonsymmetrical set of equations, yields the displacements from which the forces can be calculated by differentiation, or its equivalent, and back calculations. In the popular stiffness

method, the continuity conditions (eq. (A21)) are trivially solved by the linkage of nodal variables and condensation to generate the well-known symmetrical stiffness matrix of dimension $m \times m$, ($m = 12$ for this problem). In principle, however, equation (A23) represents the basic unabridged set of equations of the stiffness method that, for convenience, is manipulated to obtain the condensed symmetrical form.

From the structure of the IFM equations (eq. (A15)) and the stiffness equations (eq. (A23)), we observe the following:

(1) In the IFM the equilibrium equations, written in terms of forces, are augmented by the compatibility conditions, also written in terms of forces, to obtain the IFM governing equations $[\mathbf{S}]\{\mathbf{F}\} = \{\mathbf{P}^*\}$, given by equation (A15).

(2) In the stiffness method the equilibrium equations, which are expressed in terms of displacements, are augmented by displacement continuity conditions to obtain the stiffness method's governing matrix equation $[\mathbf{K}]\{\mathbf{X}\} = \{\mathbf{P}^\alpha\}$, given by equation (A23).

(3) For this problem the number of IFM governing equations (eq. (A15)) is 18, which is fewer than the 24 equations (eq. (A23)) of the displacement method.

(4) Typically, a sparser system of equations results from writing equilibrium equations in terms of forces rather than in terms of displacement variables.

(5) Both the compatibility conditions ($[\mathbf{C}][\mathbf{G}]\{\mathbf{F}\} = \{\delta\mathbf{R}\}$) of the IFM and the continuity conditions ($[\mathbf{C}\tau\gamma]\{\mathbf{X}_c\} = \{0\}$) of the stiffness method yield very sparse systems of equations; however, the equations of the continuity conditions are relatively more sparse than those of the compatibility conditions.

(6) The equilibrium equations remain indeterminate when expressed either in terms of forces or in terms of displacements (refer to IFM eq. (A16) and stiffness eq. (A20)). However, the indeterminancy of the equilibrium equations is alleviated in the case of the IFM by the compatibility condition ($[\mathbf{C}][\mathbf{G}]\{\mathbf{F}\} = \{\delta\mathbf{R}\}$), or in the displacement method by the displacement continuity condition $[\mathbf{C}\tau\gamma]\{\mathbf{X}_c\} = \{0\}$.

Appendix B
Symbols

$[\mathbf{B}]$	$(m \times n)$ equilibrium matrix
$[\mathbf{B}_e]$	element equilibrium matrix
$[\mathbf{C}]$	$(r \times n)$ compatibility matrix
$[\mathbf{C}_e]$	(3×9) elemental boundary compatibility matrix for the edge where $y = k$; $[\mathbf{C}_e] = [\mathbf{C}][\mathbf{G}]$
$[\mathbf{C}_{\tau\gamma}]$	displacement continuity matrix
E	Young's modulus
$\{\mathbf{F}\}$	internal forces; $(n \times 1)$ internal force vector
$[\mathbf{F}_k]$	force component
$[\mathbf{G}]$	$(n \times n)$ concatenated flexibility matrix
$[\mathbf{G}_e]$	element flexibiity matrix
$[\mathbf{G}_j]$	$(n \times m)$ force coefficient matrix
h	plate thickness
$[\mathbf{J}]$	deformation coefficient matrix; first $(m \times n)$ partition of $[[\mathbf{S}]^{-1}]^{\mathrm{T}}$
$[\mathbf{K}]$	$(m \times m)$ symmetrical stiffness matrix
$[\mathbf{K}_s]$	matrix defined by first $(m \times m)$ partition of $[[\mathbf{S}][\mathbf{G}]^{-1}[\mathbf{S}]^T]$
ℓ, m	direction cosines to the outward normal to the boundary curve
M_x, M_y, M_{xy}	plate bending moments; generalized stress resultants
m	number of displacement degrees of freedom
$[\mathbf{N}]$	interpolating polynomials for strain and stress
N_x, N_y, N_{xy}	generalized stress resultants
n	number of force degrees of freedom, unknown number of equations or forces in IFM
$\{\mathbf{P}\}$	$(m \times 1)$ external load vector
$\{\mathbf{P}^*\}$	equivalent loads
q	transverse distributed load
r	number of compatibility conditions, $r = n - m$
$[\mathbf{S}]$	$(n \times n)$ IFM governing matrix
U_c	complementary strain energy
U_{dis}	discretized internal energy for flexural response
U_{pb}	strain energy in flexure
V_y	shear force at any location along span of beam
w	potential of loads
$\frac{\partial^2 w}{\partial x^2}, \frac{\partial^2 w}{\partial y^2}, \frac{\partial^2 w}{\partial x \partial y}$	plate curvatures
$\{\mathbf{X}\}$	nodal displacment unknown
$\{\mathbf{X}_e\}$	concatenation of 2 elemental nodal displacements
$X_1, X_2 \ldots, X_{12}$	displacement degrees of freedom
α_1, α_2	constants linked to nodal displacement degrees of freedom
$\{\beta\}$	$[\mathbf{G}]\{\mathbf{F}\}$
$\{\beta_0\}$	$(n \times 1)$ initial deformation vector
$\gamma_{xy}, \gamma_{yz}, \gamma_{xz}$	generalized deformation
$\{\delta\mathbf{R}\}$	$(r \times 1)$ initial deformation vector; $\delta\mathbf{R} = -[\mathbf{C}]\{\beta_o\}$
δ_y	displacement at tip of beam
δ_z	transverse displacement at center of plate
$\{\epsilon\}$	strain vector
ϵ_x, ϵ_y	generalized deformations
κ	curvature
$\kappa_z, \kappa_y, \kappa_{xy}$	generalized deformations
ν	Poisson's ratio; 0.3
$\{\sigma\}$	stress vector
τ_{xy}	shear stress
ϕ, ψ	stress functions in flexure
ψ_z	transverse rotation
Ω	plate domain in Cartesian coordiantes
$[0]$	null matrix

Superscript:

T	transpose of matrix or vector

References

1. MSC/NASTRAN. A.V. Merrad, ed, The MacNeal-Schwendler Corp., Los Angeles, CA, 1981.
2. Argyris, J.H.: ASKA—Automatic System for Kinematic Analysis. Nucl. Eng. Des., vol. 6, no. 4, Aug. 1969, pp. 441-455.
3. Nakazawa, S.: The MHOST Finite Element Program, Vol-II; User's Manual, NASA CR-182235-Vol-2 1989.
4. Patnaik, S.N.: An Integrated Force Method for Discrete Analysis. Int. J. Numer. Methods Eng., vol. 6, no. 2, 1973, pp. 237-251.
5. Patnaik, S.N.: The Variational Energy Formulation for the Integrated Force Method. AIAA J., vol. 24, no. 1, Jan. 1986, pp. 129-137.
6. Patnaik, S.N.: Integrated Force Method Versus the Standard Force Method. Comput. and Struct., vol. 22, no. 2, 1986, pp. 151-163.
7. Patnaik, S.N.; Berke, L.; and Gallagher, R.H.: Integrated Force Method Versus Displacement Method for Finite Element Analysis, NASA TP-2937, 1990.
8. Patnaik, S.N.; Berke, L.; and Gallagher, R.H.: Compatibility Conditions of Structural Mechanics for Finite Element Analysis. NASA TM-102413, 1990.
9. Patnaik, S.N.; and Yadagiri, S.: Frequency Analysis of Structures by the Integrated Force Method. J. Sound Vibr., vol. 83, July 1982, pp. 93-109.
10. Patnaik, S.N.; and Joseph, K.T.: Generation of the Compatibility Matrix in the Integrated Force Method. Comput. Methods Appl. Mech. Eng., vol. 55, no. 3, May 1986, pp. 239-257.
11. Patnaik, S.N.; and Joseph, K.T.: Compatibility Conditions from Deformation Displacement Relationship. AIAA J., vol. 23, no. 8, Aug. 1985, pp. 1291-1293.
12. Patnaik, S.N.; and Yadagiri, S.: Design for Frequency by the Integrated Force Method. Comput. Methods Appl. Mech. Eng., vol. 16, no. 2, Nov. 1978, pp. 213-230.
13. Patnaik, S.N.; and Gallagher, R.H.: Gradients of Behaviour Constraints and Reanalysis via the Integrated Force Method. Int. J. Numer. Methods Eng., vol. 23, no. 12, 1986, pp. 2205-2212.
14. Patnaik, S.N.; and Nagaraj, M.S.: Analysis of Continuum by the Integrated Force Method. Comput. Struct., vol. 26, no. 6, 1987, pp. 889-905.
15. Nagabhusanam, J.; and Patnaik, S.N.: General Purpose Programme to Generate Compatibility Matrix for the Integrated Force Method. AIAA J., vol. 28, no. 10, 1990, pp. 1838-1842.
16. Vijayakumar, K.; Murty, A.V.K.; and Patnaik, S.N.: A Basis for the Analysis of Solid Continua by the Integrated Force Method. AIAA J., vol. 26, no. 5, May 1988, pp. 626-629.
17. Patnaik, S.N.; and Satish, H.: Analysis of Continuum Using Boundary Compatibility Conditions of Integrated Force Method. Comput. Struct., vol. 34, no. 2, 1990, pp. 287-295.
18. Patnaik, S.N.: Behaviour of Trusses With Stress and Displacement Constraints. Comput. Struct., vol. 22, no. 4, 1986, pp. 619-623.
19. Patnaik, S.N.: Analytical Initial Design for Structural Optimization via the Integrated Force Method., Comput. Struct., vol. 33, no.1, 1989, pp. 265-268.
20. Love, A.E.H.: A Treatise on the Mathematical Theory of Elasticity. Dover, New York, 1944.
21. Timoshenko, S.: History of Strength of Materials. McGraw-Hill, New York, 1953.
22 Whipple, S.: A Work on Bridge Building. Utica, New York, 1847.
23. Denke, P.H.: A General Digital Computer Analysis of Statically Indeterminate Structures. NASA TN D-1666, 1959.
24. Przemieniecki, J.S.; and Denke, P.H.: Joining of Complex Substructures by the Matrix Force Method. J. Aircraft, vol. 3, no. 3, May-June, 1966, pp. 236-243.
25. Kaneko, I.; Lawo, M.; and Thierauf, G.: On Computational Procedures for the Force Method. Int. J. of Numer. Methods Eng., vol. 18, no. 10, 1982, pp. 1469-1495.
26. Plemmons, R.J.: A Parallel Block Iterative Scheme Applied to Computations in Structural Analysis. SIAM J. Algebraic Discrete Methods, vol 7, no. 3, 1986, pp. 337-347.
27. Heath, M.T.; Plemmons, R.J.; and Ward, R.C.: Sparse Orthogonal Schemes for Structural Optimization Using the Force Method. SIAM J. of Sci. Stat. Comput., vol. 15, no. 3, Sept. 1984, pp. 514-532.
28. Robinson, J.: Automatic Selection of Redundancies in the Matrix Force Method: The Rank Technique. Canadian Aeronautics J., vol. 11, no. 1, Jan. 1965, pp. 9-12.
29. Przemieniecki, J.S.: Theory of Matrix Structural Analysis. McGraw-Hill, New York, 1968.
30. McGuire, W.; and Gallagher, R.H.: Matrix Structural Analysis. Wiley, New York, 1979.
31. Argyris, J.H.; and Kelsey, S.: Matrix Force Method of Structural Analysis With Applications to Aircraft Wings, Wissenschaften Gessellschaft Luftfahrt Jahrbuch, 1956, pp. 78-98.
32. Pian, T.H.H.; and Chen, D.P.: Alternative Ways for Formulation of Hybrid Stress Elements, Int. J. Numer. Methods Eng., vol. 18, no. 11, 1984, pp. 1679-1684.
33. Saleeb, A.F.; and Chang, T.Y.: An Efficient Quadrilateral Element for Plate Edition, Finite Element Method, 4th edition, O.C. Zienkiewicz and R.L. Taylor, eds., McGraw-Hill, New York, 1989, Chapt. 12-13.
34. Noor, A.K.: Multifield (Mixed and Hybrid) Finite Element Models. State-of-the-Art Surveys on Finite Element Technology, A.K. Noor and W.D. Pilkey, eds., ASME, New York, 1983, pp. 127-162.
35. Nakazawa, S.: MHOST, MARC Corp., Palo Alto, CA, NASA CR-182235.
36. On Hu-Washizu (augmented) Variational Principle. The Finite Element Method, 4th Edition, vol. 1, O.C. Zienkiewicz and R.L. Taylor, eds, McGraw-Hill, New York, 1989, Chapt. 12-13.
37. Zienkiewicz, O.C.; Kui, Li Xi-; and Nakazawa, S.: Dynamic Transient Analysis by a Mixed, Iterative Method. Int. J. Numer. Methods Eng., vol. 23, no. 7, 1986, pp. 1343-1353.
38. Felippa, C.; and Militello, C.: Developments in Variational Methods for High Performance Plate and Shell Elements. Analytical and Computational Models of Shells, A.K. Noor, T. Belytschko, and J.C. Simo, eds., ASME, New York, 1989, pp. 191-215.
39. Stress Recovery at Grid Points. MSC NASTRAN Applications Manual, J.A. Joseph, ed., MacNeal-Schwendler Corporation, 1982, Section 2.2.
40. Sokolnikoff, I.S.: Mathematical Theory of Elasticity, 2nd edition, McGraw-Hill, New York, 1956.
41. Timoshenko, S.: Theory of Plates and Shells. McGraw-Hill, New York 1959.
42. MacNeal, R.H.; and Harder, R.L.: A Proposed Standard Set of Problems to Test Finite Element Accuracy. Finite Elements in Analysis and Design, vol. 1, no. 1, Apr. 1985, pp. 3-20.
43. Smirnov, V.I.: A Course of Higher Mathematics, vol. 2, Advanced Calculus, Pergamon Press, New York, 1964.

REPORT DOCUMENTATION PAGE

Form Approved
OMB No. 0704-0188

1. AGENCY USE ONLY (Leave blank)	2. REPORT DATE	3. REPORT TYPE AND DATES COVERED
	April 1992	Technical Paper

4. TITLE AND SUBTITLE

Improved Accuracy for Finite Element Structural Analysis via a New Integrated Force Method

5. FUNDING NUMBERS

WU-505-63-5B

6. AUTHOR(S)

Surya N. Patnaik, Dale A. Hopkins, Robert A. Aiello, and Laszlo Berke

7. PERFORMING ORGANIZATION NAME(S) AND ADDRESS(ES)

National Aeronautics and Space Administration
Lewis Research Center
Cleveland, Ohio 44135-3191

8. PERFORMING ORGANIZATION REPORT NUMBER

E-5638

9. SPONSORING/MONITORING AGENCY NAMES(S) AND ADDRESS(ES)

National Aeronautics and Space Administration
Washington, D.C. 20546-0001

10. SPONSORING/MONITORING AGENCY REPORT NUMBER

NASA TP-3204

11. SUPPLEMENTARY NOTES

Surya N. Patnaik, Ohio Aerospace Institute, 2001 Aerospace Parkway, Brook Park, Ohio 44142. Dale A. Hopkins, Robert A. Aiello, and Laszlo Berke, NASA Lewis Research Center. Responsible person, Surya N. Patnaik, (216) 433-8368.

12a. DISTRIBUTION/AVAILABILITY STATEMENT

Unclassified - Unlimited
Subject Category 39

12b. DISTRIBUTION CODE

13. ABSTRACT *(Maximum 200 words)*

Finite element structural analysis based on the original displacement (stiffness) method has been researched and developed for over three decades. Although today it dominates the scene in terms of routine engineering use, the stiffness method does suffer from certain deficiencies. Various alternate analysis methods, commonly referred to as the mixed and hybrid methods, have been promoted in an attempt to compensate for some of these limitations. In recent years two new methods for finite element analyses of structures, within the framework of the original force method concept, have been introduced. These are termed the "integrated force method" and the "dual integrated force method." A comparative study was carried out to determine the accuracy of finite element analyses based on the stiffness method, a mixed method, and the new integrated force and dual integrated force methods. The numerical results were obtained with the following software: MSC/NASTRAN and ASKA for the stiffness method; an MHOST implementation for a mixed method; and GIFT for the integrated force methods. For the cases considered, the results indicate that, on an overall basis, the stiffness and mixed methods present some limitations. The stiffness method typically requires a large number of elements in the model to achieve acceptable accuracy. The MHOST mixed method tends to achieve a higher level of accuracy for coarse models than does the stiffness method as implemented by MSC/NASTRAN and ASKA. The two integrated force methods, which bestow simultaneous emphasis on stress equilibrium and strain compatibility, yield accurate solutions with fewer elements in a model. The full potential of these new integrated force methods remains largely unexploited, and they hold the promise of spawning new finite element structural analysis tools.

14. SUBJECT TERMS

Finite element method; Stiffness; Solid mechanics; Plates; Flexibility

15. NUMBER OF PAGES

28

16. PRICE CODE

A03

17. SECURITY CLASSIFICATION OF REPORT	18. SECURITY CLASSIFICATION OF THIS PAGE	19. SECURITY CLASSIFICATION OF ABSTRACT	20. LIMITATION OF ABSTRACT
Unclassified	Unclassified	Unclassified	

NSN 7540-01-280-5500

Standard Form 298 (Rev. 2-89)
Prescribed by ANSI Std. Z39-18
298-102

NASA-Langley, 1992